

NUMERICAL STUDY OF CONCURRENT FLAME SPREAD OVER AN
ARRAY OF THIN DISCRETE SOLID FUELS

by

JEANHYUK PARK

Submitted in partial fulfillment of the requirements

For the degree of Master of Science

Department of Mechanical and Aerospace Engineering

CASE WESTERN RESERVE UNIVERSITY

January, 2018

Case Western Reserve University

School of Graduate Studies

We hereby approve the thesis¹ of

JEANHYUK PARK

for the degree of

Master of Science

Defense Date: 06.07.2017

Dr. Ya-Ting T. Liao

Committee Chair, Adviser
Department of Mechanical and Aerospace Engineering

Date

Dr. James T'ien

Committee Member
Department of Mechanical and Aerospace Engineering

Date

Dr. Paul J. Barnhart

Committee Member
Department of Mechanical and Aerospace Engineering

Date

Dr. Fumiaki Takahashi

Committee Member
Department of Mechanical and Aerospace Engineering

Date

¹We certify that written approval has been obtained for any proprietary material contained therein.

Table of Contents

List of Tables	v
List of Figures	vi
Abstract	xii
Chapter 1. Introduction	1
Upward Flame Spread	1
Discrete Fuel Configuration	2
Approach	5
Chapter 2. Method	6
Model Description	6
Governing Equations	10
2.2.1. Mass and Species Transport	11
2.2.2. Energy Conservation and Velocity Divergence	12
2.2.3. Radiation	14
2.2.4. Momentum Transport	15
2.2.5. Transport Coefficients for DNS	16
2.2.6. Combustion	17
2.2.7. Solid Heat Conduction and Pyrolysis	18
Numerical Setup	19
2.3.1. Solution Procedure	19
Chapter 3. Buoyancy Driven Flame in 1-g	22
General Trend of Upward Flame Spread in 1-g	22
	iii

Characteristics of Buoyancy Driven Flame Spread across Discrete Fuel Samples in	
1-g	25
Comparison between Continuous and Discrete Fuel Samples	27
3.3.1. Pyrolysis and Burning Rate	27
3.3.2. Gas and Solid Profiles	30
Net Heat, Burning Rate, and Preheated Length	33
Chapter 4. Concurrent Forced Flame in 0-g	37
Characteristics of Concurrent Flame Spread across Discrete Fuel Samples in 0-g	37
Comparison between Continuous and Discrete Fuel Samples	42
4.2.1. Pyrolysis and Burning Rate	42
4.2.2. Gas and Solid Profiles	44
Net Heat, Burning Rate, and Preheated Length	46
Chapter 5. Analysis	48
Comparison between 1-g and 0-g	48
Grid Setup	52
Chapter 6. Conclusions	56
Appendix A. FDS Input Codes	59
1-g Input Code	59
0-g Input Code	96
Appendix. Complete References	116

List of Tables

2.1	Fuel-Gap configurations simulated in 1-g	8
2.2	Thermophysical properties of gas and solid phase	8
2.3	Fuel-Gap configurations simulated in 0-g	10
5.1	Number of grid used in Fine Grid and Coarse Grid simulation. The resulting grid dimensions are listed on the bottom two rows.	54
5.2	Qualitative grid analysis comparing average pyrolysis spread rate at different grid resolution	55

List of Figures

2.1	1-g simulation set up	7
2.2	0-g simulation set up	10
3.1	Flame tip, flame base, and flame length vs time for continuous fuel configuration in 1-g	24
3.2	Evolution of temperature contours for flame spread across discrete fuel samples. Length of each fuel sample: 1cm. Separation distance: 1.5cm. Black contour: heat release rate =15,000 kW/m ³ .	25
3.3	Flame base position vs time for different fuel-gap configurations.	27
3.4	Pyrolysis front and base locations vs. time for continuous fuel sample and the net heat flux on the sample surface for discrete fuel samples (gap length = 1.5-cm). The adjusted locations are the locations minus the total length of the gap upstream.	29
3.5	Flame shapes (heat release rate =15,000kW/m ³) for discrete (1.5-cm gap) and continuous fuel configurations at t = 4s. The continuous and discrete fuel sample locations are denoted by the orange and black boxes respectively on the left	30
3.6	Flame shape (heat release rate =15,000 kW/m ³), velocity field, and solid profiles at t = 4s	31
3.7	Selected solid phase properties of 1-g simulations integrated over virgin fuel length. Blue trace is the continuous configuration and orange line is 1.5-cm gap configuration	34

3.8	Selected solid phase properties of 1-g simulations integrated over virgin fuel length. Blue trace is the continuous configuration and orange line is 1.5-cm gap configuration	35
4.1	Evolution of temperature contours for flame spread across discrete fuel samples. Length of each fuel sample: 1cm. Separation distance: 1.5cm. Black contour: heat release rate =15,000 kW/m ³ .	38
4.2	Flame location vs time for selected fuel configurations in 0-g	40
4.3	Flame base position vs time for different fuel-gap configurations.	41
4.4	Pyrolysis front and base locations vs. time for continuous fuel sample and discrete (gap length = 1.5-cm) fuel samples . The adjusted locations are the locations minus the total length of the gap upstream.	42
4.5	Flame shapes (heat release rate =15,000kW/m ³), and vector plot for discrete 1.5-cm gap (left) and continuous fuel configurations (right) at t = 6.1 s.	44
4.6	Comparison of selected solid phase properties from left to right (Net Heat Flux, Burning Rate, Non-dimensional Area Density) of continuous (red lines) and discrete fuel (blue lines) in 0-g simulations at selected times.	45
4.7	Time evolution of selected solid phase properties of 0-g simulations integrated over virgin fuel length. Blue trace is the continuous configuration and orange line is 1.5-cm gap configuration	46
5.1	A side-by-side comparison between the flame profile and vector plot in 0-g (left) and 1-g (right)	49

5.2	Comparison of different modes of heat flux, flame profile, and surface density at selected instances	50
5.3	Selected solid phase properties of 0-g and 1-g simulations integrated over unburned fuel length. Blue trace is the continuous configuration and orange line is 1.5-cm gap configuration	52
5.4	Grid Dependency Study on different configurations. The blue lines are finer grid simulation and the red lines are regular, coarse grid result.	53

Latin Characters

A	Pre-exponential factor in gas phase reaction	
c_p	Specific Heat	(kJ/kg/K)
$D_{\alpha,\beta}$	Diffusion coefficient for species α diffusing into species β	(m^2/s)
E	Activation energy	(kJ/mol)
e	Specific internal energy	(kJ/kg)
\mathbf{F}	Force vector	(N)
\mathbf{f}_b	Body Force	(N)
g	Gravity	(m/s^2)
H	Modified pressure	(m^2/s^2)
h	Specific enthalpy	(kJ/kg)
h_s	Sensible enthalpy	(kJ/kg)
δh_c^0	Heat of combustion	(kJ/kg)
\mathbf{I}	Radiation intensity	($W/m^2/sr$)
I_b	Blackbody radiation intensity	($W/m^2/sr$)
k	Thermal conductivity	($W/m/K$)
L_f	Fuel length	(m)
L_g	Length of the gap	(m)
\dot{m}''_{α}	Mass flux of species α	($kg/m^2/s$)
\dot{m}'''_{α}	Mass production rate of species α per unit volume	($kg/m^3/s$)
n_w	Normal vector to the wall	
\tilde{p}	Flow induced perturbation pressure	(Pa)
\bar{p}	Mean background pressure	(Pa)

p_0	Ambient pressure	(Pa)
Pr	Prandtl Number	
$\dot{\mathbf{q}}''$	Heat flux vector	(kW/m ²)
\dot{q}_b'''	Heat release rate per unit volume	(kW/m ³)
\dot{q}_c''	Convective heat flux	(kW/m ²)
\dot{q}_r''	Radiative heat flux	(kW/m ²)
R	Universal gas constant	(J/K/mol)
r_s	Solid phase reaction rate	(mol/L/s)
S	Area	(m/s)
\mathbf{s}'	Unit direction vector of radiation intensity	
$S_{i,j}$	Rate of strain tensor	(1/s)
T	Temperature	(K)
T_0	Ambient Temperature	(K)
t	Time	(s)
u	Fluid velocity in x direction	(m/s)
\mathbf{u}	Velocity vector	(m/s)
$v_{pf,avg}$	The average pyrolysis base spread rate	(m/s)
$v_{pf,avg}$	The average pyrolysis front spread rate	(m/s)
W	Molecular Weight	(g/mol)
w	Velocity in z-direction	(m/s)
w_0	Forced air velocity in z-direction	(m/s)
Y_α	Mass fraction of species α	
Z_α	Mole fraction of species α	
z_{total}	Total fuel span (fuel + gap)	

z_p	Total fuel span (fuel + gap)	
z_{pyro}	The pyrolysis position at t	(m)

Greek Characters

α	Species α	
β	Species β	
κ	Mean absorption coefficient	(1/m)
μ	Dynamic viscosity	(kg/m/s)
ν_g	Gas yield in pyrolysis reaction	
ν_α	Stoichiometric coefficient of species α	
ρ	Density	(kg/m ³)
ρ'	Surface Density	(kg/m ²)
ρ'_0	Initial surface density value	(kg/m ²)
ρ^*	Non-dimensional surface density	
σ	Stefan-Boltzmann constant	(W/m ² /K ⁴)

Abstract

Numerical Study of Concurrent Flame Spread over an Array of Thin Discrete Solid Fuels

Abstract

by

JEANHYUK PARK

Building fire, Forrest fire, and warehouse compartment fire are some of the most frequently occurring practical fire hazards in modern world. Although these types of hazards seem irrelevant from one another, they have some things in common from the perspective of fire protection engineering, in that they all have a very similar fundamental fuel-gap configuration, or discrete fuel configuration. There has been some studies in the past regarding the subject, yet it is not the most popular in the field. Furthermore, there is even fewer, if not any, numerical analysis done to fires in discrete fuel configuration. Discrete fuel arrangements represent some practical fire hazard situations, such as compartment fires in enclosed vehicles. In this study, an unsteady two-dimensional numerical model (Fire Dynamics Simulator) was used to simulate concurrent flame spread over paper-like thin solid fuels in discrete configurations in microgravity (0g, where a 20cm/s flow is imposed) and in normal gravity (1g). An array of ten 1cm-long fuel segments is uniformly distributed in the flow direction (0g) or in the vertical direction (1g). A hot spot ignition source is applied at the upstream leading edge of the first fuel segment. The separation distance between the fuel segments is a parameter in this study,

ranging from 0 (corresponding to a continuous fuel) to 3cm. Using this setup, the spread rate of the flame base and the fuel burning rate were studied. The spread rate in 1g and 0g increases with increasing separation distance. This is due to the gaps in the discrete fuel that force the flame base to jump to the subsequent fuel segment when the upstream segment burns out. On the other hand, the fuel burning rate behaves differently in 1g versus 0g. At a flow velocity of 20 cm/s in 0g, the flame reaches a limiting length and the flame length is approximately the same (4cm) for all fuel configurations. Therefore, as the separation distance increases, the preheating length (the fuel area exposed to the flame) decreases, resulting in a smaller burning rate. In 1g, the buoyancy driven flow accelerates as it rises, resulting in a longer flame as the separation distance increases. In all simulated configurations, the flame extends to the last fuel segment before the first fuel segment burns out and the flame spans the entire set of fuel segments. However, flame standoff distance reduces at the gaps between fuel segments, and in some configurations, the flame breaks into multiple flamelets. The shorter standoff distance and intense burning at each flamelet base result in a larger total burning rate as the separation distance increases.

1 Introduction

1.1 Upward Flame Spread

Upward flame spread over solid fuels in 1-g has been widely researched by many in the field of combustion and fire science. Flame spread over solid can be broken down into two main processes. In the first process, a solid fuel is exposed to a heat flux above certain values, the fuel undergoes a local phase change from solid to a gaseous state, and releases combustible fuel vapor. This process is commonly known as pyrolysis. In the second process, the fuel vapor is mixed with oxygen at the right ratio and, when the temperature is high enough to overcome the activation energy, the mixture undergoes exothermic chemical reactions, also known as combustion. This process is ignition. After ignition, if the gas-phase combustion is able to provide the thermal energy to continue the heating/pyrolysis process of the solid fuel, which in turn releases fuel vapor to sustain the gas combustion, a diffusion flame will form and will be able to grow and spread over the solid fuel.

A concurrent flow is flow in the direction in which the flame spread. An opposed flow is the flow in the opposite direction. In 1-g, flame is affected by the natural convection due to the gravity and the flow is driven by the buoyant force. Upward flame spread in 1-g (concurrent flow in 1-g) grows much faster than the downward flow (opposed

flow in 1-g). This is because in upward flame spread, the flame covers the unburned solid fuel, facilitating the aforementioned interactions between the flame and the fuel. [1]-[6] While upward flame spread has extensively been studied by Quintiere[1]-[2] and Fernades-Pello[4]-[7], the application of this on complex or non-homogeneous geometry is relatively new.

1.2 Discrete Fuel Configuration

Discrete (or discontinuous) fuel configuration consists of multiple fuel segments separated by inerts or air gaps. In many practical situations, discrete fuel better represents the fuel load arrangement. For example, wildland forest trees, urban buildings, commodities stored in warehouses, and balconies in multi-story apartment buildings represent discrete combustible elements. Flame spread across discrete fuel can have very different characteristics from that of continuous fuel. The presence of spaces between the combustibles can serve as barriers and decrease the probability of flame spread [8, 11]. However, when the flame does spread, the spread rate for discrete fuels can be higher than for continuous fuels. Many works suggest that the flame spread rate increases when the fuel element separation distance increases [12], or when the fuel loading (mass per volume) decreases [13]. Some works suggest that there is an optimal fuel percentage (or porosity) for flame spread [11, 14]. This means that the fire concern for the discrete fuel elements can be more extreme compared with continuous fuels. Therefore, understanding the spreading phenomenon over the discrete fuel is crucial for fire safety consideration.

Previous studies investigated flame spread across discrete elements in the horizontal plane with or without forced convection [8],[11],[13],[15]-[16]. For example, Vogel and Williams [15] performed experiments of flame propagation along a horizontal array of vertically oriented matchsticks (with the heads removed). They explored the propagation boundary in terms of matchstick height and separation distance. A theoretical model was also proposed based on a constant ignition temperature and previously-obtained flame standoff profile. Agreement between the theory and the experiment suggested that convective effects are of primary importance in flame propagation at matchstick size scales. Prahl and T'ien [16] studied flame spread across vertically oriented matchsticks in the presence of forced convection. The imposed wind was up to three feet per second, blowing with or against the direction of fire spread. They presented the necessary conditions for flame propagation in a non-dimensional plot of S/L (separation distance and matchstick height ratio) vs. W/U (wind velocity non-dimensionalized by natural convection velocity). Watanabe et al [11] conducted an experiment of flame spread along thin combustible solid (filter paper) with randomly distributed pores. They defined a scale ratio S as the ratio of pore size to the pre-heat length ahead of the flame leading edge. Their results showed that for $S \leq 1$, the flame spread rate increases with porosity and reaches a maximum value at approximately 20-30% porosity. For $S > 1$, the spread rate is almost constant up to 40% porosity. Over 40% porosity, the spread rate decreases with increasing porosity and reaches 0 beyond 60% for both $S \leq 1$ and $S > 1$.

Some researchers introduced single array or multiple parallel arrays of discrete fuel elements on an inclined plane [17], [18]. Weber [17] followed Vogel and Williams [15] and proposed a geometrical model for flame spread over vertically mounted fuel arrays

on an inclined base. The flame propagation speed is expressed in terms of three quantities: 1) the flame spread rate for vertical (downward) propagation on a single element, 2) the flame strength parameter, and 3) the base inclination angle. Based on the model, there exists a critical inclination angle at which heat transfer processes cease to be a limiting factor in fire propagation. Finney et al [18] examined the fire spread thresholds in a discrete fuel bed with inclination. The control parameters included the vertical fuel-bed depth (height), the horizontal spacing between fuel elements, and the slope of the fuel bed arrays. They concluded that the fire spread occurred only after ignition by direct flame contact. Also, they found that fires were more likely to spread in deeper beds and with steeper slopes.

Upward flame spread across vertical discrete fuel elements were also studied [12, 14]. Goller et al [12] performed experiments on upward flame spread across vertical arrays of horizontally protruding wood matchsticks. They investigated the influence of separation distance (the spacing between the fuel elements) on flame spread, time to burnout, and mass-loss rates. They performed analyses based on convective heat-transfer correlations and droplet burning theory (extended for a cylindrical geometry) to predict the ignition time (and spread rate), the burning time, and the mass loss rate. Their experimental results were consistent with their predictions, suggesting that convective heat transfer is the mechanism controlling ignition at this small (matchstick) scale. Miller and Gollner [14] conducted experiments on upward flame spread over vertical arrays of alternating lengths of PMMA and insulation. They found that the flame spread rate peaks at around 67-89% fuel percentage (ratio of the fuel length to the total length), and that there is a fuel percentage limit below which the flame fails to spread. They also proposed a model to estimate the flame spread rate at different fuel percentages with

knowledge of the homogeneous fuel spread rate and a reasonable assumption for the limiting fuel percentage.

While some researches, including but not limited to aforementioned studies, have provided insights on how flame propagates in discrete fuel configuration, a few of them provided explanation on what causes faster flame spread in certain discrete fuels. In addition, Most of those studies are experimental, and are very limited in measuring certain important parameters such as flow velocity and heat flux. On the other hand, a comprehensive numerical study will provide valuable data that leads to the complete understanding of this process.

1.3 Approach

In this work, upward flame spread over thin fuel will be numerically examined, with several discrete and one continuous fuel configurations. The relationship between spread rate and discrete fuel configuration will be discussed in two different flow situations: concurrent flow under forced flow velocity of 20 cm/s in 0-g and buoyancy driven flow in 1-g. The objective of this work is to (1) numerically evaluate the effect of gaps on the flame spread process (2) extensively examine certain gas and solid phase profiles such as flow velocity field, solid surface density, and burning rate, and (3) determine the dominating factors of the flame spread rate.

2 Method

2.1 Model Description

1-g: Buoyancy Driven Flow

Upward flame spread across discrete thin fuel samples is numerically simulated in this work. All simulations are performed using Fire Dynamics Simulator (FDS) 6.2.0, revision 22352. FDS is an open source CFD code for low-speed flow, with an emphasis on smoke and heat transfer from fire. It is mainly developed by NIST and VTT, Finland. The FDS input code is based on Erik Stalkup's simulation on flame spread over thin corrugated solid [9], with modifications on boundary conditions and model geometry. The complete input codes used for this study can be found in appendix A.

The model configuration in 1-g is shown in Fig. 2.1. An array of 10 fuel samples is placed vertically. The fuel samples are separated by gaps of air. The length of each fuel sample is 1cm, resulting in 10-cm of total fuel length. To clarify some terminologies, the total fuel length refers to the sum of the lengths of the fuels, which is different from total fuel span in the Fig. The total fuel span refers to the total length of the fuel and gap combined, ranging from the bottom of the lowest fuel segment to the top of the highest fuel segment. The total fuel length is kept constant in all fuel-gap configurations to keep the fuel mass constant throughout different simulations. A total of 6 simulations

is performed, where distance between samples is varied from 0-cm (continuous setup) to 3-cm. Table 2.1 lists the fuel-gap configuration and its total fuel span.

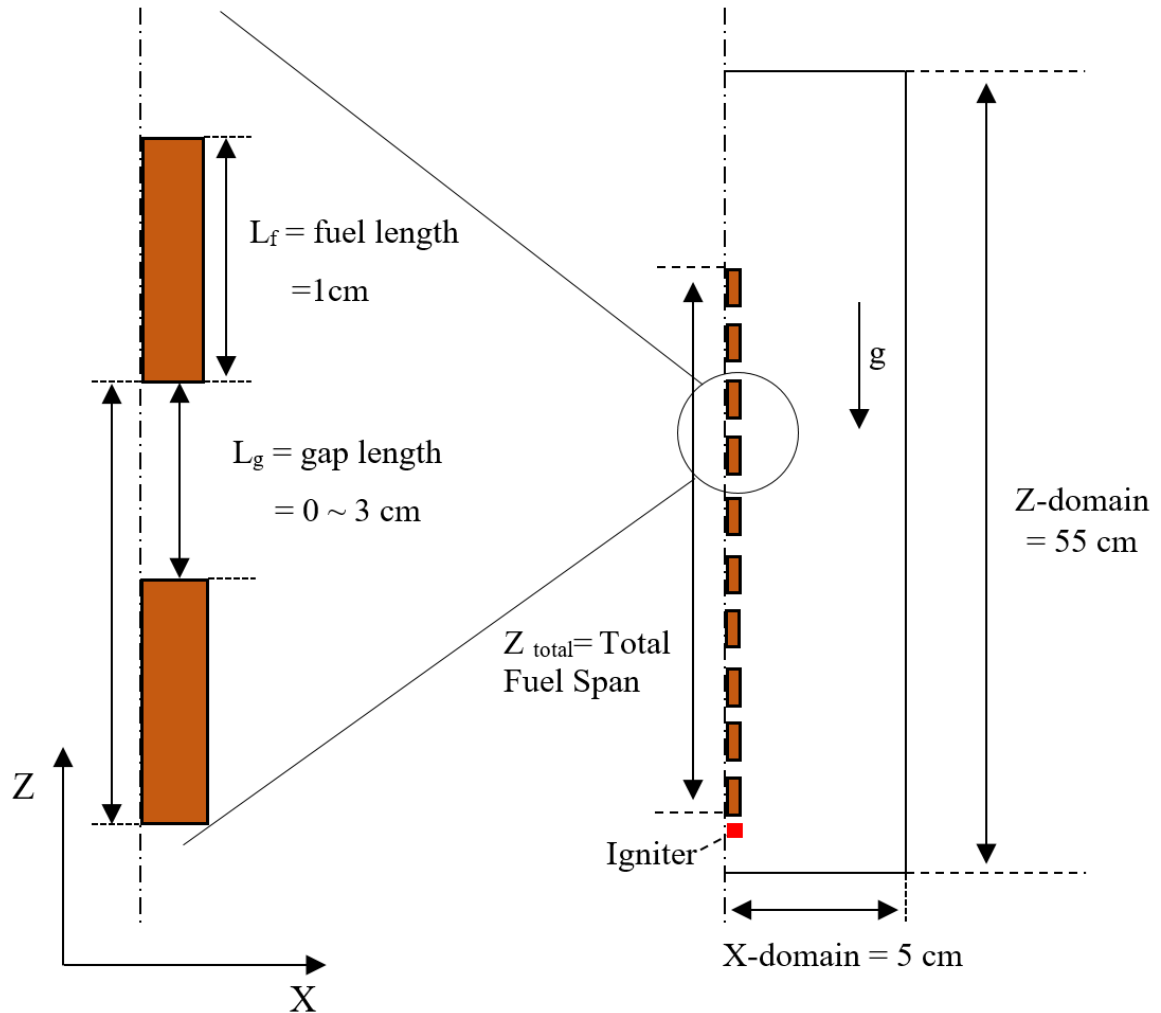


Figure 2.1. 1-g simulation set up

The fuel sample is modeled after Whatman filter paper with material properties of cellulose. The filter paper's thickness is measured to be 0.23 mm. In the numerical model, the fuel is assumed to yield 10% chemically inert char during the combustion process. The ignition is achieved by prescribing high temperature to a hotspot, which is located 1 mm below the first sample (a red square labeled as "Igniter" in Fig. 2.1). The

Table 2.1. Fuel-Gap configurations simulated in 1-g

Type	Gap Length (cm)	Total Fuel Span (cm)
Continuous	0	10
Discrete	0.25	12.25
Discrete	0.399	13.591
Discrete	0.6	15.4
Discrete	1	19
Discrete	1.5	23.5
Discrete	3	37

surface temperature of the hotspot is maintained at 1000 °C for three seconds starting at $t = 0$, and is removed at $t = 3$ seconds.

Two-dimensional Direct Numerical Simulations (DNS) is performed, including one-step finite-rate gas-phase combustion, one-step first-order solid Arrhenius pyrolysis, and gray gas radiation modeling for all gas species. The details of the DNS equations and solution procedures of FDS can be found in FDS technical References[?] documents and are summarized in section 2.2. The gas and solid thermophysical properties, gas-phase reactions, and solid pyrolysis model used in this work are the same as those in Stalkup's work. [9]

Table 2.2. Thermophysical properties of gas and solid phase

Gas Phase				Solid Phase			
Property	Value	Units	Ref.	Property	Value	Units	Ref.
A	4.23×10^{14}	$\text{cm}^3/\text{g/s}$	[24]	A_s	1.00×10^{10}	1/s	[24]
E	1.13×10^5	kJ/kmol	[24]	$c_{p,s}$	1.20×10^5	kJ/kg/K	[26]
Δh_c^0	1.58×10^4	kJ/kg	[25]	E_s	1.25×10^5	kJ/kg	[24]
\bar{p}_0	101,352	Pa		Δh_c^0	751.8	kJ/kg	[24]
P_r	0.7			k_s	101,352	Pa	[26]
T_0	293	K		ϵ	1		[28]
ν_g	0.9			$\rho_{s,0}$	555.3	kg/m^3	[27]

In order to save computational time, the half-thickness sample plane (dash-dot-line in Fig. 2.1) is assumed to be symmetric. Therefore, only half of the flow domain is simulated and half of the solid thickness is used. On the symmetric plane, free-slip and no flux boundary condition are assumed at the air gaps. In addition, on the back side of the solid on the symmetry plane, adiabatic condition is applied. The computational domain ranges from 0 to 55cm in the fuel length direction (z axis, where $z = 4$ cm corresponds to the bottom edge of the first fuel sample) and from 0 to 5 cm in the fuel thickness direction (x axis, where $x = 0$ cm corresponds to the sample half-thickness). The grid size is $\delta_x = 0.7576mm$ and $\delta_z = 1.421mm$, resulting in $66 \times 387 = 25,542$ grids.

Lastly, the boundary condition for the domain is set such that it is similar to that of the intended experiment design - open on all sides and the top, while bottom is closed due to the proximity to the sample holder table. In terms of 2-D simulation model, open boundaries are prescribed to x -max and z -max plane. This means that the air can flow freely in and out x -max ($x=5$ cm) and z -max ($z = 55$ cm) domain. Numerically, open boundary means upwind boundary condition where the values of the species mass fractions and temperatures are taken from either the adjacent values for incoming flow, and nearest grid cell value for outgoing flow[20].

0-g: Forced Convective Flow

The model configuration in 0-g is shown in figure 2.2. In 0-g simulation, all simulation conditions and models are identical to 1-g simulation except that forced flow at 20 cm/s is applied in the fuel length direction (z -axis) A total of 3 simulations are performed at different fuel-gap combinations. Table 2.3 lists the fuel-gap configuration and its total fuel span.

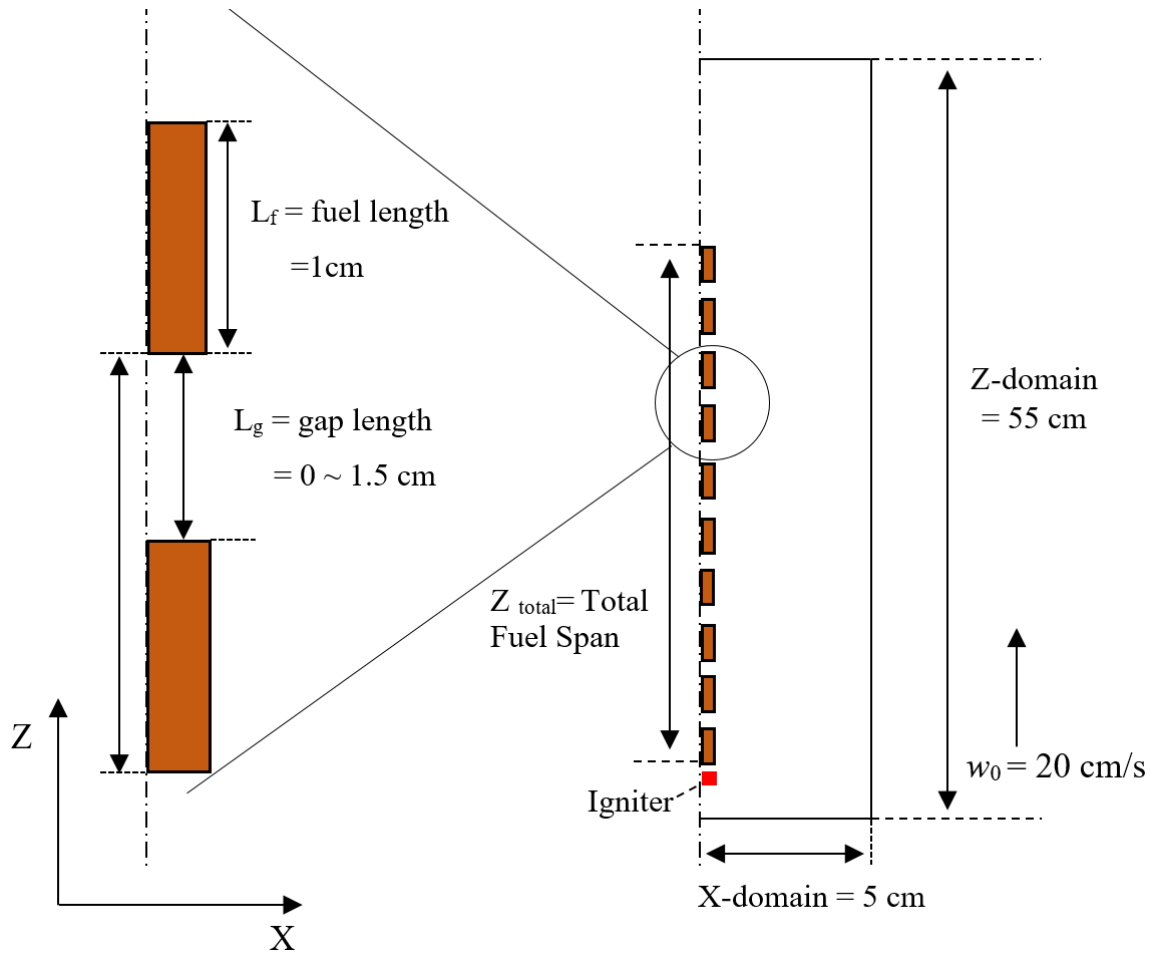


Figure 2.2. 0-g simulation set up

Type	Gap Length (cm)	Total Fuel Span (cm)
Continuous	0	10
Discrete	0.6	15.4
Discrete	1.5	19

Table 2.3. Fuel-Gap configurations simulated in 0-g

2.2 Governing Equations

FDS numerically solves simplified Navier-Stokes Equations in three dimension. It is suitable for fire driven flow at low Mach number. For this study, DNS is implemented for the simulation. The detailed solution procedures and the theory behind can be found

in FDS Technical References[20] document. In this subsection, the governing equations used in DNS are summarized. The governing equations are expressed in general 3-D differential form. However, the actual simulation in this work is performed in two dimension.

2.2.1 Mass and Species Transport

The transport equation for species α can be written as

$$\frac{\partial}{\partial t}(\rho Y_\alpha) + \nabla \cdot (\rho Y_\alpha \mathbf{u}) = \nabla \cdot (\rho D_\alpha \nabla Y_\alpha) + \dot{m}_\alpha''' + \dot{m}_{b,\alpha}''' \quad (2.1)$$

where Y_α is the mass fraction of species α , ρ is the density, and \mathbf{u} is the velocity vector. There are two source terms generated from chemical equation where \dot{m}_α''' is the mass production rate of species α , and $\dot{m}_{b,\alpha}'''$ is the mass production rate of α by evaporating droplets or particles. It is assumed that in any combustion process, Nitrogen is the dominant species, therefore the diffusion coefficient, $D_{\alpha,\beta}$, of a species α diffusing into Nitrogen is used in the species mass transport equations

$$(\rho D)_{\alpha,DNS} = \rho D_{\alpha,N_2}$$

By assuming $\sum \rho D_\alpha \nabla Z_\alpha = 0$ and realizing $\sum \dot{m}_\alpha''' = 0$, the mass transport equation can be obtained by summing Eq. (2.1)

$$\frac{\partial \rho}{\partial t} + \nabla \cdot (\rho \mathbf{u}) = \dot{m}_b''' \quad (2.2)$$

where the mass density is obtained from $\rho = \sum (\rho Y)_\alpha$.

For pressure approximation in low Mach number application, Rehm and Baum's approach [10] is used, where pressure is obtained by summing background pressure, $\bar{p}(z, t)$, and flow-induced perturbation pressure, $\tilde{p}(\mathbf{x}, t)$.

$$p(x, t) = \bar{p}(z, t) + \tilde{p}(\mathbf{x}, t) \quad (2.3)$$

The background pressure can be calculated by the ideal gas law

$$\bar{p} = \rho T R \sum_{\alpha} \frac{Y_{\alpha}}{W_{\alpha}} \equiv \frac{\rho R T}{\bar{W}} \quad (2.4)$$

The low Mach number assumption serves two purposes. First, it filters acoustic waves, which means the time step is not bound by speed of sound but the flow speed. The second purpose is that this approach can reduce the number of dependent variables of the systems of equations to one, velocity divergence, and allows velocity divergence to be able to solved by thermodynamic variables. This will be explained in detail in the next section.

2.2.2 Energy Conservation and Velocity Divergence

As a result of low Mach number assumption, the enthalpy, h , is dependent on internal energy, e , and background pressure, in the form of $h = e + \bar{p}/\rho$. The conservation of energy equation in terms of sensible enthalpy, h_s , then becomes

$$\frac{\partial}{\partial t}(\rho h_s) + \nabla \cdot (\rho h_s \mathbf{u}) = \frac{D\bar{p}}{Dt} + \dot{q}''' - \dot{q}_b''' - \nabla \cdot \dot{\mathbf{q}}'' \quad (2.5)$$

Here, \dot{q}''' is heat release rate per unit volume from chemical reaction and \dot{q}_b''' is the heat loss to the subgrid droplets and particles. The operator D/Dt denotes material derivative.

The term $\dot{\mathbf{q}}''$ represents total heat flux from conduction, diffusion, and radiation:

$$\dot{\mathbf{q}}'' = -k\nabla T - \sum_{\alpha} h_{s,\alpha} \rho D_{\alpha} \nabla Y_{\alpha} + \dot{\mathbf{q}}_r'' \quad (2.6)$$

where k is thermal conductivity. Rather than solving the equation explicitly, Eq. 2.5 is implicitly solved for the velocity divergence and can be rearranged using sensible enthalpy

$$\nabla \cdot \mathbf{u} = \frac{1}{\rho h_s} \left[\frac{D}{Dt} (\bar{p} - \rho h_s) + \dot{q}''' - \dot{q}_b''' - \nabla \cdot \dot{\mathbf{q}}'' \right] \quad (2.7)$$

Expanding Eq. 2.7 for m th zone with background pressure at m th zone, \bar{p}_m , will result in the following equation

$$\nabla \cdot \mathbf{u} = D - P \frac{\partial \bar{p}_m}{\partial t} \quad (2.8)$$

where

$$P = \frac{1}{\bar{p}_m} - \frac{1}{\rho c_p T} \quad (2.9)$$

and

$$\begin{aligned} D = & \frac{1}{\rho c_p T} [\dot{q}''' - \dot{q}_b''' - \nabla \cdot \dot{\mathbf{q}}'' - \mathbf{u} \cdot \nabla (\rho h_s) + w \rho_0 g_z] \\ & + \frac{1}{\rho} \sum_{\alpha} \left(\frac{\bar{W}}{W_{\alpha}} - \frac{h_{s,\alpha}}{c_p T} \right) \left[\nabla \cdot (\rho D_{\alpha} \nabla Y_{\alpha}) - \mathbf{u} \cdot \nabla (\rho Y_{\alpha}) + \dot{m}_{\alpha}''' + \dot{m}_{b,\alpha}''' \right] \end{aligned} \quad (2.10)$$

The time derivative of the background pressure of m th zone can be obtained by integrating Eq. 2.8 over the zone volume, Ω_m ,

$$\frac{\partial \bar{p}_m}{\partial t} = \left(\int_{\Omega_m} D dV - \int_{\partial\Omega_m} \mathbf{u} \cdot d\mathbf{S} \right) / \int_{\Omega_m} P dV \quad (2.11)$$

Since the D term at the next zone is solvable with thermodynamic variables and \mathbf{u} at current zone is known, the time derivative of the pressure is obtainable, which can be used to calculate the velocity divergence from Eq. 2.8

2.2.3 Radiation

By default, FDS uses gray assumption, which means the net radiation energy is gained by absorption and emission, but not scattering. For gray gas, the radiative heat flux gradient, $\nabla \cdot \dot{\mathbf{q}}_r''$, from Eq. 2.6 can be written as

$$-\nabla \cdot \dot{\mathbf{q}}_r''(\mathbf{x}) = \kappa(\mathbf{x})[U(\mathbf{x}) - 4\pi I_b(\mathbf{x})] \quad ; \quad U(\mathbf{x}) = \int_{4\pi} I(\mathbf{x}, \mathbf{s}') d\mathbf{s} \quad (2.12)$$

The term $\kappa(\mathbf{x})$ is the local absorption coefficient which is tabulated at the beginning of the simulation for each radiation band. $I_b(\mathbf{x})$ is the fraction of the blackbody radiation at temperature, $T(\mathbf{x})$, and can be expressed as

$$I_b = \frac{F_n(\lambda_{min}, \lambda_{max})\sigma T(\mathbf{x})^4}{\pi} \quad (2.13)$$

where F_n is the view factor and, if the spectral dependence is lumped into one coefficient, $F_n = 1$. Multiplied by the absorption coefficient, κ , it makes up the absorption term in the radiative flux. The radiation intensity $I(\mathbf{x}, \mathbf{s})$ can be written as

$$I(\mathbf{x}, \mathbf{s}) = \int_{4\pi} I(\mathbf{x}, \mathbf{s}') d\mathbf{s}' \quad (2.14)$$

where \mathbf{s} is the direction of intensity. Combined with κ , $I(\mathbf{x}, \mathbf{s})$ makes up the radiation emission source term.

2.2.4 Momentum Transport

The non-conservative form of momentum equation takes the form of

$$\rho \left(\frac{\partial \mathbf{u}}{\partial t} + (\mathbf{u} \cdot \nabla) \mathbf{u} \right) + \nabla p = \rho \mathbf{g} + \mathbf{f}_b + \nabla \cdot \boldsymbol{\tau}_{ij} \quad (2.15)$$

where \mathbf{f}_b is the drag force exerted by particles and droplets. The viscous stress tensor $\boldsymbol{\tau}_{ij}$ can be expressed in terms of dynamic viscosity, μ , Kroneker delta, δ_{ij} , and symmetric strain tensor, S_{ij}

$$\tau_{ij} = 2\mu S_{ij} - \frac{2}{3}\mu S_{kk}\delta_{ij} \quad ; \quad S_{ij} \equiv \frac{1}{2} \left(\frac{\partial u_i}{\partial x_j} + \frac{\partial u_j}{\partial x_i} \right) \quad , \quad i, j, k = 1, 2, 3 \quad (2.16)$$

Using low Mach approximation, subtracting hydrostatic pressure gradient, and applying vector identity, Eq. 2.15 can be rewritten as

$$\frac{\partial \mathbf{u}}{\partial t} - \mathbf{u} \times \boldsymbol{\omega} + \nabla H - \tilde{p} \nabla \left(\frac{1}{\rho} \right) = \frac{1}{\rho} \left[(\rho - \rho_n) \mathbf{g} + \mathbf{f}_b + \nabla \cdot \boldsymbol{\tau}_{ij} \right] \quad (2.17)$$

where $\boldsymbol{\omega}$ is the vorticity vector and H is defined as $H \equiv |\mathbf{u}|^2/2 + \tilde{p}/\rho$. Eq. 2.17 can be simplified as

$$\frac{\partial \mathbf{u}}{\partial t} + \mathbf{F} + \nabla H = 0 \quad (2.18)$$

The vector \mathbf{F} is referred as the momentum flux term and it contains the cross product of velocity and vorticity, drag force vector, and divergence of viscous stress tensor terms.

By taking the divergence of Eq. 2.18, Poisson equation for the pressure is obtained

$$\nabla^2 H = - \left[\frac{\partial}{\partial t} (\nabla \cdot \mathbf{u}) + \nabla \cdot \mathbf{F} \right] \quad (2.19)$$

2.2.5 Transport Coefficients for DNS

In Direct Numerical Simulati (DNS) on where grid size is small enough, the thermo-dynamic and molecular properties such as viscosity, thermal conductivity, and mass diffusivity, can be used directly. The values of μ , k , and D can be approximated from kinetic theory and are dependent on temperature. The viscosity of species α is

$$\mu_{\alpha} = \frac{26.69 \times 10^{-7} (W_{\alpha} T)^{\frac{1}{2}}}{\sigma_{\alpha}^2 \Omega_{\nu}} \quad [=] \quad \text{kg}/(\text{m} \cdot \text{s}) \quad (2.20)$$

where σ_{α} is the Lennard-Jones hard-sphere diameter (\AA) and Ω_{ν} is the collision integral. The thermal conductivity of species α is

$$k_{\alpha} = \frac{\mu_{\alpha} c_{p,\alpha}}{Pr} \quad [=] \quad \text{W}/(\text{m} \cdot \text{s}) \quad (2.21)$$

where the default Prandtl number is set as 0.7. The viscosity and thermal conductivity can be calculated by multiplying the individual species value to its mass fraction and summing the products.

$$\mu_{DNS} = \sum_{\alpha} Y_{\alpha} \mu_{\alpha} \quad ; \quad k_{DNS} = \sum_{\alpha} Y_{\alpha} k_{\alpha} \quad (2.22)$$

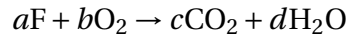
the diffusion coefficient of species α diffusing into species β is

$$D_{\alpha\beta} = \frac{2.66 \times 10^{-7} T^{3/2}}{W_{\alpha\beta}^{1/2} \sigma_{\alpha\beta}^2 \Omega_D} \quad [=] \quad \text{m}^2/\text{s} \quad (2.23)$$

where $W_{\alpha\beta} = 2/(1/W_{\alpha} + 1/W_{\beta})$, $\sigma_{\alpha\beta} = (\sigma_{\alpha} + \sigma_{\beta})/2$, and Ω_D is the diffusion collision integral. As previously mentioned, the diffusion coefficient of any species is assumed to be diffused in the nitrogen, which is a dominating species in combuston.

2.2.6 Combustion

For a given species α , the mass fraction, Y_α , mass flux source term \dot{m}_α''' , and heat release rate per unit volume, \dot{q}''' can be calculated by combustion modeling. A one step, second order, finite rate chemistry is used for combustion model. In a standard one step, Fuel-Oxygen chemical reaction



Here, the rate expression for a species α , r_α follows Arrhenius law

$$r_\alpha = \left(\frac{\nu_\alpha}{\nu_F}\right) AT^n C_F C_{O_2} e^{E_\alpha/RT} \quad (2.24)$$

where A is a preexponential factor of the reaction, E_α is the activation energy, R is the gas constant, (ν_α/ν_F) is the stoichiometric ratio of α and the fuel. n is the temperature exponent and 0 is used for the value of this particular simulation. The concentration fraction C_α is

$$C_\alpha = \frac{Y_\alpha \rho}{W_\alpha} \quad (2.25)$$

where W_α is the molecular weight of species α . Once the rate of species is calculated, the source terms from species Eq. 2.1 and energy Eq. 2.5 can be obtained. The mass per unit volume of the species α is

$$\dot{m}_\alpha''' = W_\alpha r_\alpha \quad (2.26)$$

and the heat release rate per unit volume is

$$\dot{q}''' = \Delta h_c^\circ \dot{m}_F''' \quad (2.27)$$

where Δh_c° is heat of combustion for fuel.

2.2.7 Solid Heat Conduction and Pyrolysis

FDS uses one-dimensional (x-direction) heat conduction equation to solve solid phase temperature, T_s . Since this study deals with a very thin fuel and conduction within the fuel is assumed to have negligible effect, 1-D conduction is deemed sufficient. The heat equation for solid is

$$\rho_s c_{p,s} \frac{\partial T_s}{\partial t} = \frac{\partial}{\partial x} \left(-k_s \frac{\partial T_s}{\partial x} \right) + \dot{q}_s'' \quad (2.28)$$

where subscript s denotes solid properties. The source term \dot{q}_s'' consists of chemical and radiative source terms

$$\dot{q}_s'' = \dot{q}_{s,c}'' + \dot{q}_{s,r}'' \quad (2.29)$$

The chemical source term, $\dot{q}_{c,s}''$, is heat loss to the solid fuel due to pyrolysis. The radiative source term consists of radiation and wall radiation loss

$$\dot{q}_{s,r}'' = \dot{q}_{r,in}'' + \dot{q}_{r,out}'' = \int_{s', \mathbf{n}_w < 0} I_w(\mathbf{s}') |\mathbf{s}' \cdot \mathbf{n}_w| d\Omega + \epsilon \sigma T_w^4 \quad (2.30)$$

where T_w is the wall temperature. The boundary condition for solid-gas interphase is characterized as

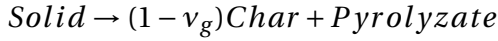
$$-k_s \frac{\partial T_s}{\partial x}(0, t) = \dot{q}_c'' + \dot{q}_r'' \quad (2.31)$$

where the convective term in DNS is characterized by

$$\dot{q}_c'' = -k_s \frac{\partial T}{\partial n} = k_s \frac{T_w - T_g}{\delta n/2} \quad (2.32)$$

where T_g is the gas phase temperature and n is the grid space normal to the surface.

Solid reactions in FDS is modeled under the following assumption that 1) gas species are released instantaneously, 2) the solid and gaseous components are in local thermal equilibrium, 3) there is no condensation from gas products, and 4) there is no porosity effect. A one step simple pyrolysis follows the following reaction



where ν_g is the gas yield fraction and can be specified by users. Reactions with $\nu_g < 1$ is modeled to leave a chemically inert char. The rate of pyrolysis reaction follows Arrhenius law

$$r_\alpha = \left(\frac{\rho_{s,\alpha}}{\rho_{s,\alpha}(0)} \right) A e^{E_\alpha/RT_s} \quad (2.33)$$

where $\rho_{s,\alpha}/\rho_{s,\alpha}(0)$ is the ratio of solid density to initial solid density, and T_s is the surface temperature. The rate of mass turning from solid to gas phase (pyrolyzate) per unit volume, $\dot{m}_{\alpha,g}'''$ can be expressed as

$$\dot{m}_{\alpha,g}''' = \rho_{\alpha,s}(0) \nu_g r_\alpha \quad (2.34)$$

The chemical source term (heat loss to the solid) in Eq. 2.29 becomes

$$\dot{q}_{s,c}'' = -\rho_{\alpha,s}(0) r_\alpha \Delta h_r \quad (2.35)$$

2.3 Numerical Setup

2.3.1 Solution Procedure

FDS uses time-marching, two-stage Runge-Kutta scheme to solve reacting flow. It follows a predictor-corrector method where the species and the source terms are solved

after the corrector step of transport equations. The followings are a brief summary of predictor-corrector steps. Both are solved within the same time step before marching in time.

Predictor Step:

1) The thermodynamic variables and species (ρ , (ρY_α) , Y_α , \bar{W} , \bar{p} , and T) are solved using mass, species transport equation and the equation of state (Eq. 2.2, 2.1, and 2.4)

2) The velocity divergence from Eq. 2.8 is calculated, by first computing D from Eq. 2.10 and $\partial \bar{p}_m / \partial t$ using Eq. 2.11.

3) Using the velocity divergence from the previous step, the Poisson equation from Eq. 2.19 is solved to obtain Bernoulli integral, H .

4) The velocity field is calculated and updated using Eq. 2.18. The solution procedure is designed such that the velocity divergence from Eq. 2.8 is guaranteed to be matched with velocity field solved in Eq. 2.18.

Corrector Step:

1) Similar procedure to predictor step (1) is repeated. However, when setting up the variables at " n " th time step to solve for the variables at " $n+1$ " th time step, the " n " th time step variables are averaged with the values obtained from the predictor step. For instance, to solve for density using discretized Eq. 2.2 at " $n+1$ " th time step

$$\rho^{n+1} = \frac{1}{2}(\rho^* + \rho^n) - \frac{\Delta}{2} \left[\frac{\delta(\bar{\rho} u_i)^*}{\delta x_i} \right] \quad (2.36)$$

where the subscript "*" represents the values obtained from predictor step.

2) Solve the temperature, species, and heat source terms ((ρY_α) , Y_α , \bar{W} , T , and \bar{q}''') using chemical reaction equations (Eq. 2.1, 2.24, 2.26, 2.27 and 2.4)

3) The velocity divergence is calculated using Eq.2.8. Similar to corrector step (1), averaged values of predictor steps and "n" th time step is used.

4) Using the velocity divergence from the previous step, the Poisson equation from Eq. 2.19 is solved to obtain Bernoulli integral, H .

5) The velocity field is calculated and updated using Eq. 2.18.

To ensure the stability of the solution, several constraints that are variation of the Courant-Friedrichs-Lewy(CFL) condition is imposed on the time step. For diffusive transport, Von-Neumann constraint is imposed where

$$\delta t_{max} \left[\frac{\mu}{\rho}, D_{\alpha} \right] \sum_i \frac{1}{\delta x_i^2} < \frac{1}{2} \quad (2.37)$$

To account for thermal expansion, realizable mass density condition is imposed to CFL constraint where

$$\delta t < \left[\frac{\bar{u}_i}{\delta x_i} + \nabla \cdot \mathbf{u} \right]^{-1} \quad (2.38)$$

3 Buoyancy Driven Flame in 1-g

The 1-g simulation is performed with different seven different gap lengths, ranging from 0-cm (continuous) to 1.5-cm. In this chapter, we will first present the general trend of upward flame spread in 1-g using the continuous fuel case, then discuss the special characteristics of upward flame spread across discrete fuel samples. At the end we will compare both gas phase and solid phase profiles of discrete and continuous fuel configuration and analyze the different flame spread trend in both configurations

3.1 General Trend of Upward Flame Spread in 1-g

The ignition of occurs around $t = 1.45$ s in all fuel configurations. As shown in the contour plots in figure 3.2 (left and right panels), the base of the flame stays laminar due to low flow speed. The gas flows faster in the upstream direction of the flame and transitions to turbulent flow as indicated by the eddies in the flame tip area.

To visualize this transient progression of this general upward flame trend, the flame positions (tip and base) of the continuous configuration is plotted against the simulation time in the center plot of figure 3.1. Here, the flame position is tracked based on the previously mentioned HRRPUV criteria. The orange line is the base of the flame (most upstream position), yellow line is the tip of the flame (most downstream), and the blue

is the length of the flame, which can be calculated by subtracting the flame base from the flame tip.

After the ignition at around $t = 1.45$ s, the flame base position rises gradually, while the flame tip propagates at a much faster rate. Up until $t = 2.75$ s, both flame tip and base propagates at a steady rate. As shown in the left contour plot at $t = 2.75$ s, that around the time where flame length just about exceeds the length of the fuel. Along the fuel, the flow is affected by the boundary layer and the gas is slow near the fuel surface, which is why the flame length grows relatively slower. Once the flame length exceeds the fuel lengths after $t = 2.75$ s, the flame tip portion where it is no longer covered by the fuel accelerates quickly due to the buoyancy effect and the absence of the boundary layer. This can easily be visualized by the unsteady eddies in the right contour plot and rapidly fluctuating patterns in the flame tip position in the center plot of Fig. 3.1.

This general pattern of upward flame spread due to the buoyancy driven flow can be observed in all fuel configurations. However, Some unique phenomenon are shown only in discrete fuel configurations. They will be discussed in the next section

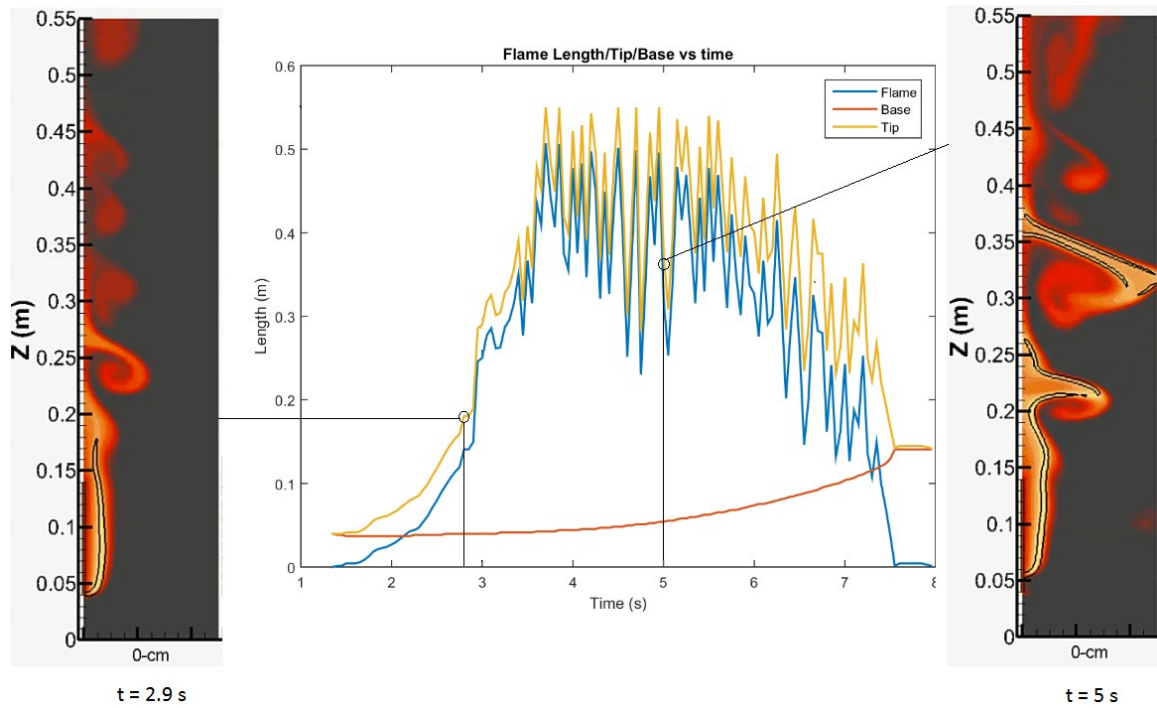


Figure 3.1. Flame tip, flame base, and flame length vs time for continuous fuel configuration in 1-g

3.2 Characteristics of Buoyancy Driven Flame Spread across Discrete Fuel Samples in 1-g

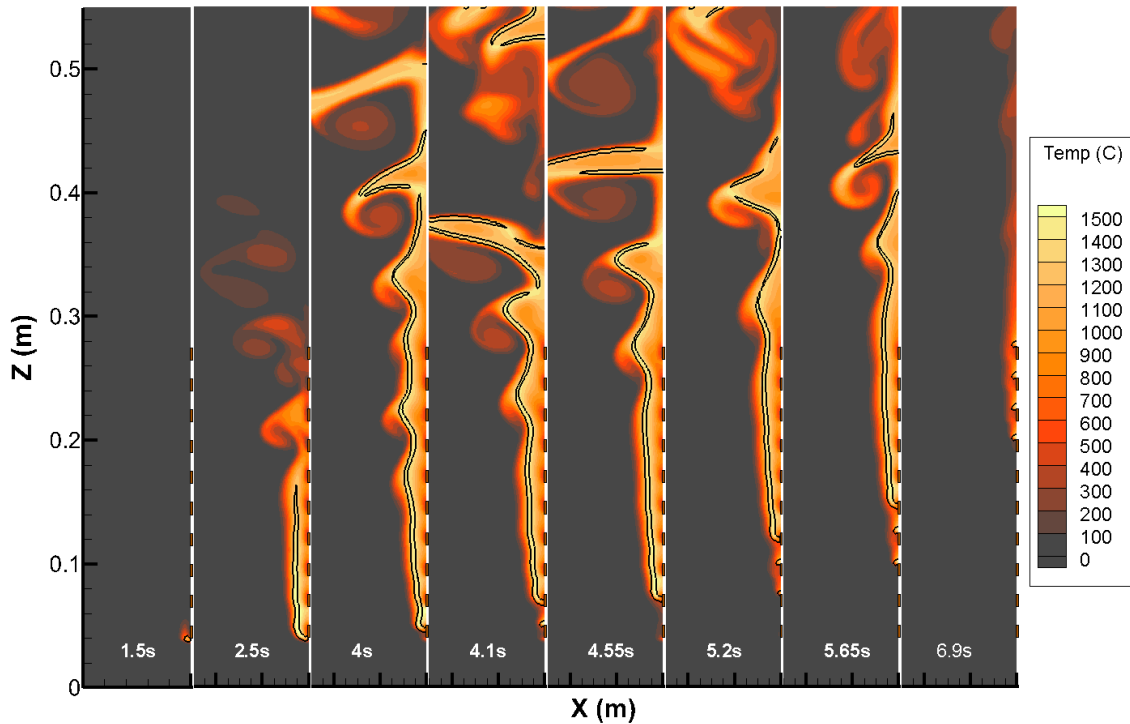


Figure 3.2. Evolution of temperature contours for flame spread across discrete fuel samples. Length of each fuel sample: 1cm. Separation distance: 1.5cm. Black contour: heat release rate = $15,000 \text{ kW/m}^3$.

To demonstrate the transient progression of flame spread over discrete fuel, 1.5-cm gap is selected as a representative configuration for discrete fuel. A simulation video that contains different fuel configurations, including continuous, is available online [22]. In this configuration, 10 identical fuel samples of 1-cm in length each are separated by 1.5-cm air gap. In Fig. 3.2, the gas temperature profile (colormap) and flame shape (black contour) are shown. Again, the flame is defined as $\text{HRRPUV} > 15,000 \text{ kW/m}^3$. Note that in Fig. 3.2, the aspect ratio of X to Z is 2:1 and the flame picture may appear to be slightly

exaggerated. The flame base location vs time is tracked in Fig. 3.3 for all simulation cases, including the continuous configuration.

As shown in the first frame in Fig. 3.2, at $t = 1.5$ s, there is a reaction kernel at the pilot hotspot location. Once a flammable gas mixture is achieved, ignition occurs and a diffusion flame is formed. At $t = 2.5 - 4$ s, the flame grows in length. During this period, the flame front advances to the end of the last fuel sample and the flame base slowly spreads up along the first fuel sample. As the flame grows longer, the downstream part of the flame shows turbulent characteristics including irregularity and eddies. At $t = 4.1$ s, flame splitting occurs: an upstream flame continues to burn the first fuel sample and a downstream flame attaches and spreads along the second fuel sample. At $t = 4.55$ s, the first fuel sample is fully consumed, the upstream flame dies, and the flame base ‘jumps’ to the next fuel sample, resulting in the stepping in Fig. 3.3.

Between $t = 4.55$ s and 5.65 s, this flame ‘splitting’ and ‘jumping’ process repeated. Sometimes, the upstream flame did not die before the downstream flame split again. In this case, multiple flamelets would be observed. At the end of the simulation, four flamelets were observed ($t = 6.9$ s in Fig. 3.2). These flamelets died sequentially after the corresponding fuel samples were fully consumed one by one (see the “stepping” in Fig. 3.3 at $t = 6.9 - 7.5$ s).

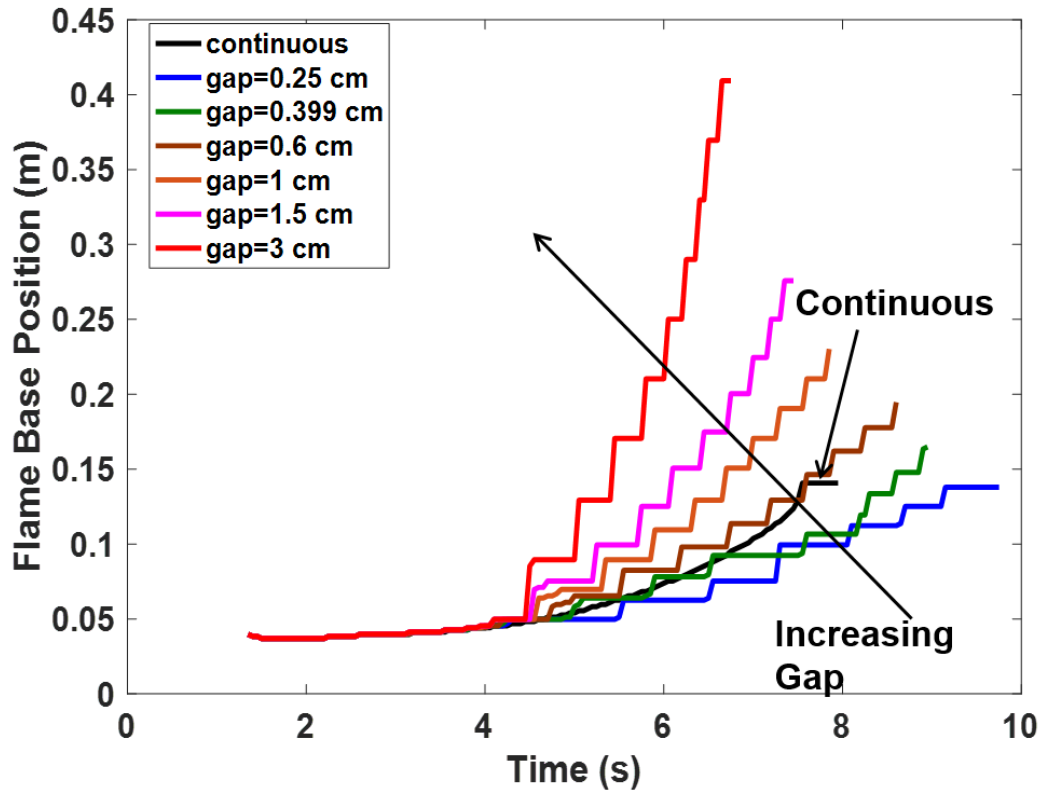


Figure 3.3. Flame base position vs time for different fuel-gap configurations.

3.3 Comparison between Continuous and Discrete Fuel Samples

3.3.1 Pyrolysis and Burning Rate

In Fig. 3.4, the location of the pyrolysis regions for the 1.5 cm fuel-percentage discrete fuel configuration is compared with the pyrolysis of the continuous fuel. The pyrolysis regions are defined as the region where the solid burning rate is larger than 0.01

$kg/s/m^2$. Initially, two other parameters are considered to be used to track pyrolysis region; non-dimensional surface density and surface temperature. However, surface temperature alone is less desirable criteria to track the pyrolysis region, as it takes some time to heat up a solid fuel, which can cause an inaccurate estimation of pyrolysis base position. Surface density requires different criteria for the pyrolysis tip and pyrolysis base. In addition, once the surface density value passes set threshold value, it is impossible to differentiate whether the solid fuel is burnt out in the pyrolysis front or not. Therefore, mass burning rate is the most reliable criteria of all three parameters considered. In Fig. 3.4, the pyrolysis front and base (the most downstream and the most upstream points of the pyrolysis regions) for the 1.5-cm gap-fuel configuration are shown as blue lines, and those for continuous fuel are shown as red lines. At a given time, the discrete fuel pyrolysis front and base are always ahead of those of the continuous fuel. In Fig. 3.4, the adjusted pyrolysis positions (black lines) were also recorded (see “Discrete Adj.” traces). The adjustment involves subtracting the total length of upstream gap from the unadjusted positions. Even when the gap length is eliminated, the entire pyrolysis process of the discrete fuel is faster than the continuous fuel by about 1 second. This means that, not only the flame not only travels faster due to the presence of physical gaps, but also actually burns faster in some discrete fuel configuration than continuous fuel.

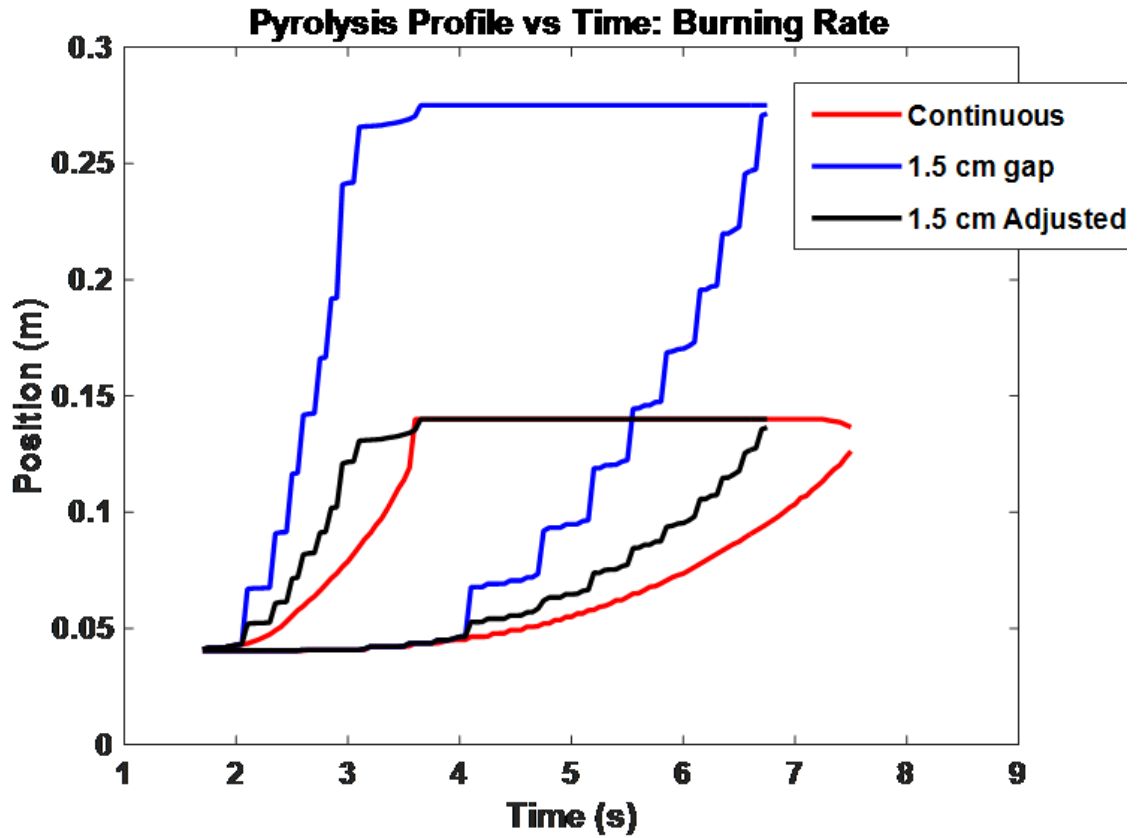


Figure 3.4. Pyrolysis front and base locations vs. time for continuous fuel sample and the net heat flux on the sample surface for discrete fuel samples (gap length = 1.5-cm). The adjusted locations are the locations minus the total length of the gap upstream.

To understand why the flame spreads faster in the discrete fuel configuration, the flame and solid profiles are examined in detail.

3.3.2 Gas and Solid Profiles

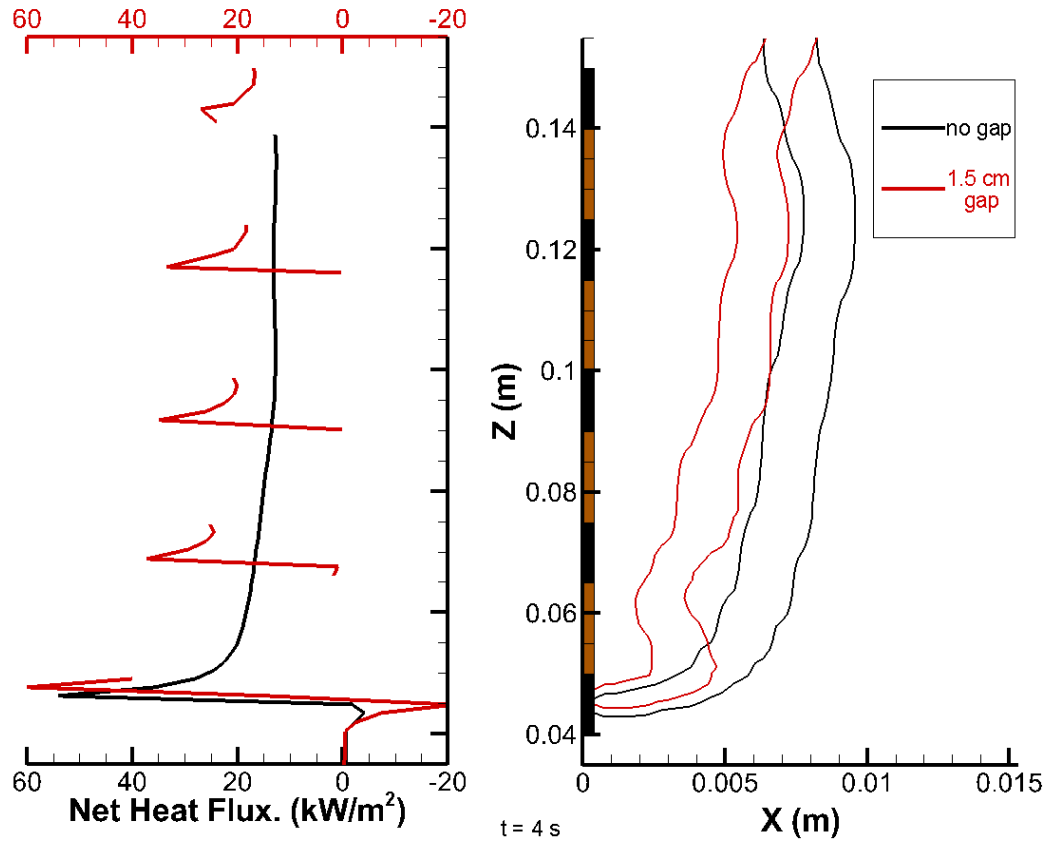


Figure 3.5. Flame shapes (heat release rate = $15,000 \text{ kW/m}^3$) for discrete (1.5-cm gap) and continuous fuel configurations at $t = 4 \text{ s}$. The continuous and discrete fuel sample locations are denoted by the orange and black boxes respectively on the left

In Fig. 3.5, the flame shapes and the net heat flux on the sample surface for continuous and discrete configurations are compared at $t = 4 \text{ s}$. The flame standoff distance, the distance between the flame and the sample surface, is shorter in the discrete fuel configuration than that for the continuous fuel.

The flow velocity, non-dimensional fuel surface density, and the fuel burning rate are further compared in Fig. 3.6. For upward flame spreading, the fuel coming out of

the sample surface needs to travel (via convection and diffusion) across the induced buoyancy flow to meet the air. Therefore the reaction zone resembles the flow boundary layer. Note that, on the other side of the flame (e.g. at $x = 0.01$ in Fig. 3.6), the air is entrained into the reaction zone, by the buoyancy flow.

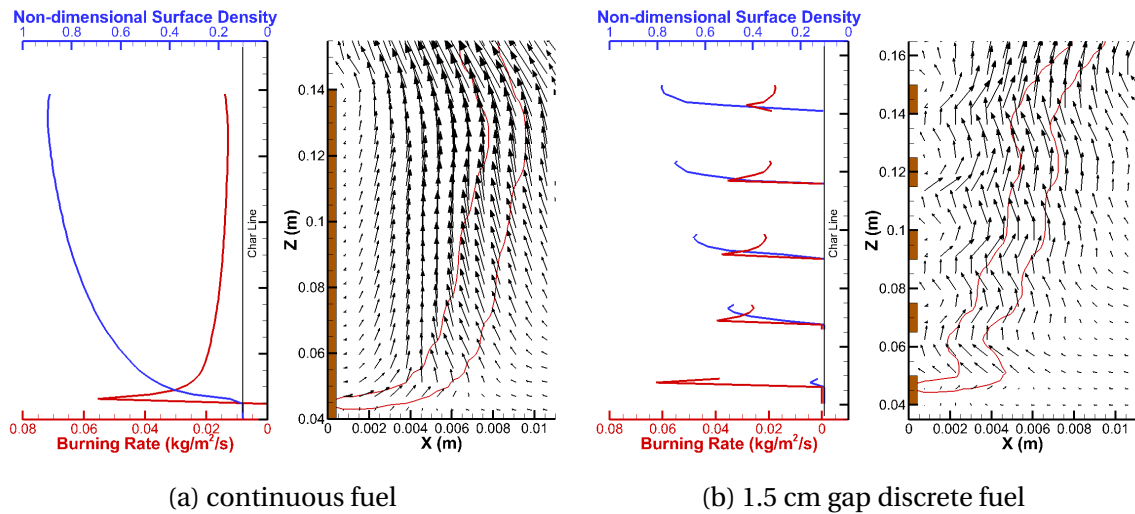


Figure 3.6. Flame shape (heat release rate = $15,000 \text{ kW/m}^3$), velocity field, and solid profiles at $t = 4 \text{ s}$

For continuous fuel sample (shown in Fig. 3.6a), the flame shape first follows the boundary layer, resulting in a growing standoff distance throughout the span of the fuel in the direction of the flow. However, near the upper end of the sample, the boundary layer ends and fuel vapor production ceases. The entrained air pushes the reaction zone towards the sample surface, resulting in a decrease of the standoff distance.

For discrete fuel configurations, this phenomenon repeats at each fuel segment. At the end of each fuel sample, the standoff distance drops. When the flame reaches the next fuel sample, the standoff distance increases again. As shown in Fig. 3.6b, this pattern repeats and the flame displays a zigzag pattern with a shorter overall standoff distance than the continuous fuel case in Fig. 3.6a.

The flame standoff distance directly affects the heat feedback from the flame to the sample surface (see Fig. 3.5), which in turn determines the burning rate of the sample. Figure 3.6a shows that for the continuous fuel, the burning rate has its largest value at the flame base, and it decreases as the standoff distance increases in the stream-wise (upward) direction. Note that in this instance, the combustible of the fuel burns out upstream (at around $z = 0.045\text{m}$), leaving 10% char behind. Similar burning rates and unburned fuel percentages are observed at each fuel segment in the discrete fuel configuration (shown in 3.6b). The surface density profile shows that the bottommost part of the second fuel segment (at around $z = 0.0675\text{ m}$) already burned out (the blue trace shows density = 0.1) while the first fuel segment is still burning. Therefore, when the first fuel segment burns out, the pyrolysis base needed to jump not only across the inter-sample gap but also across the length of fuel sample that had already burned out. In other words, the jumping distance consisted of two parts, the gap distance and the length of the burnout portion of the next sample. The reason the flame can burn out the downstream fuel segment prior to the upstream segment being completely burned is because of the non-monotonous standoff distance phenomenon presented above. In 3.6a, the maximum burning rate at the fifth fuel segment ($z = 0.145\text{m}$) is $0.025\text{ kg/m}^2/\text{s}$. This location corresponds to $z = 0.085\text{m}$ (0.045 m above the sample bottom) in the continuous fuel configuration. The burning rate at $z = 0.085\text{ m}$ for the continuous fuel is $0.015\text{ kg/m}^2/\text{s}$. The discrete fuel has a larger burning rate (and hence burns faster) because of the shorter standoff distance caused by the presence of the gaps.

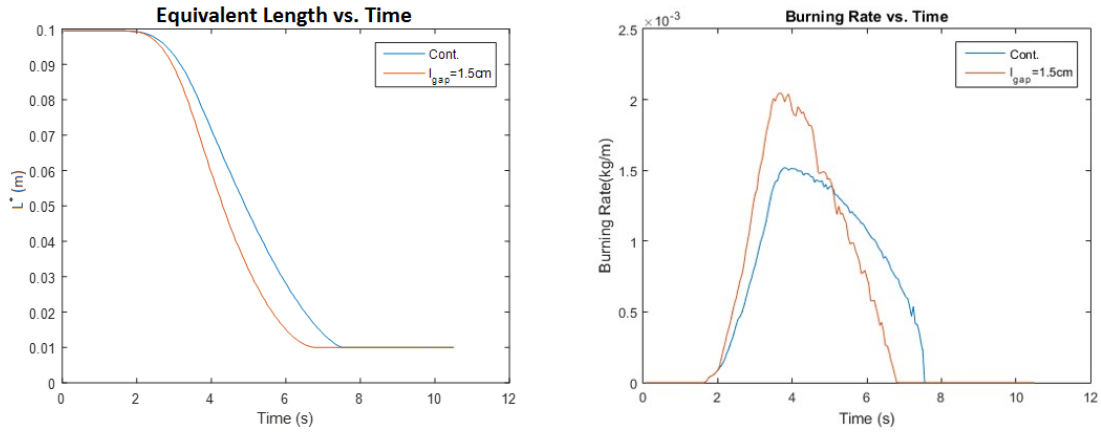
3.4 Net Heat, Burning Rate, and Preheated Length

One of the unique characteristics of discrete fuel configuration is that the fuel burns faster than continuous configuration. In order to quantify the how fast the solid fuel vaporizes, equivalent fuel length vs time ie examined. Equivalent fuel length (L^*) is defined as

$$\text{Equivalent length} = L^* = \int_{z_{fuel}} \rho^{*'} dz \quad (3.1)$$

Surface density provides the overall mass per unit area of the fuel surface. It is computed by taking integral of density over the fuel thickness. The non-dimensional surface density ($\rho^{*'}$, where the surface density, ρ' is divided by initial surface density) is numerically integrated over the fuel length - including the char - at each time instance using trapezoidal rule:

In the equivalent length vs time plot (Fig. 4.6a left), $L^{*'}$ values are identical at $t = 0$ - 2 for both continuous fuel (light blue line) and 1.5 cm gap, discrete fuel (orange line): both starts at 0.1 m and decreases at similar rate in the initial period. Then, a little after $t = 2$ s, the $\rho^{*'}$ of the discrete fuel decreases faster until the discrete fuel burns out first, as the orange line reaches 0.01 m first.



(a) Non dimensional density length vs time for (b) Burning rate per unit width vs time for continuous and 1.5-cm gap setup

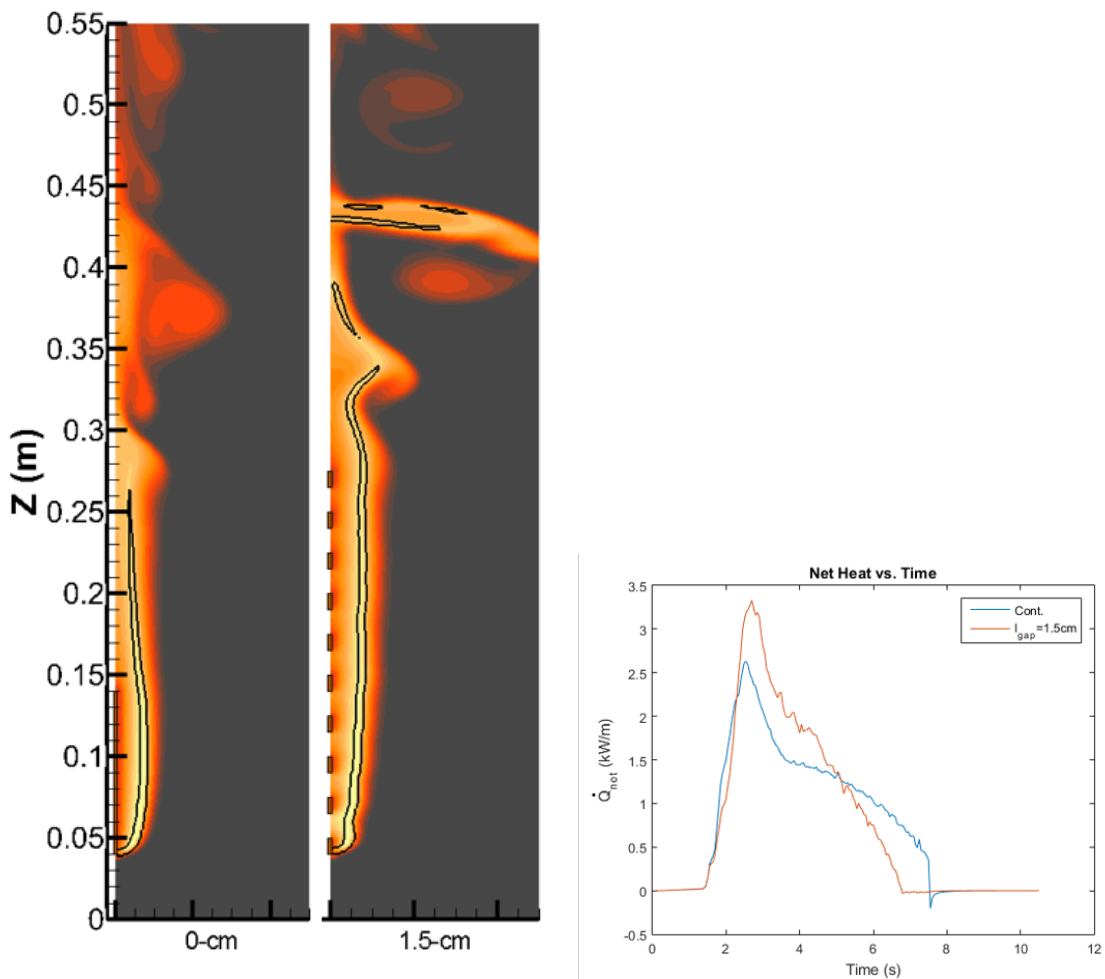
Figure 3.7. Selected solid phase properties of 1-g simulations integrated over virgin fuel length. Blue trace is the continuous configuration and orange line is 1.5-cm gap configuration

Burning rate per unit area, (m_b''), measures how fast the solid fuel vaporizes per unit area obtained by training the absolute value of the time derivative of non-dimensional density. Similar to previous analysis, burning rate per unit area is numerically integrated over the unburned fuel length to obtain an expression for burning rate per unit width (will be referred as burning rate):

$$\text{Burning Rate per unit width} = m_b' = \int_{z_{fuel}} m_b'' dz \quad (3.2)$$

Time plot (Fig. 4.6b right), the burning rate of discrete fuel (orange line) are identical to that of continuous fuel (blue line) at $t = 0 - 2$ s. Burning rates of both discrete fuel and continuous fuel increases at $t = 2 - 4$ s, but the discrete fuel burns significantly faster. This is consistent with the observation in discrete fuel simulation (Fig. 3.2), where the flame grows in full length and covers the entire fuel surfaces at $t = 2 - 4$ s.

At about $t = 4\text{s}$, both discrete and continuous fuel reaches maximum at around $m_b'' = 2 \times 10^{-3} \text{ kg/m/s}$ for discrete and about $m_b' = 1.5 \times 10^{-3} \text{ kg/m/s}$ for continuous. While the burning rate decreases for both configurations after $t=4\text{s}$, the burning rate for discrete fuel drops fast.



(a) Side by side gas phase temperature plot of continuous fuel and 1.5-cm fuel at around $t = 3.6$ where the flame exceeds total fuel span
 (b) Net heat vs time for two both configuration

Figure 3.8. Selected solid phase properties of 1-g simulations integrated over virgin fuel length. Blue trace is the continuous configuration and orange line is 1.5-cm gap configuration

Burning rate depends on total heat input onto the fuel surfaces, \dot{Q}_{net} , which depends on both \dot{q}''_{net} and $l_{preheat}$. For discrete fuel, \dot{q}''_{net} is higher than continuous fuel due to shorter flame stand-off distance. On the other hand, $l_{preheat}$ is similar in both configurations. This is because the flame covers the whole fuel span in both cases and $l_{preheat}$ is approximated by the total fuel span (0.1m in both cases). Integrating \dot{q}''_{net} over the unburned fuel surface at each time step results in the following expression:

$$\dot{Q}_{net} = \int_{l_p} \dot{q}''_{net} dz \sim \dot{q}''_{net} l_{preheat} \quad (3.3)$$

The net heat vs time plot (Fig. 3.8b) shows that after the flame reaches full length at $t = 3.15s$, \dot{Q}_{net} is noticeably higher for discrete fuel (orange line). While $l_{preheat}$ are similar for both configurations, discrete fuel has higher \dot{q}''_{net} and subjected to higher \dot{Q}_{net} , resulting in faster burning rate.

4 Concurrent Forced Flame in 0-g

The 0-g simulation is performed with four different gap lengths, from 0-cm (continuous) to 1.5-cm. In this chapter, we will first discuss the special characteristics of concurrent flame spread across discrete fuel samples in 0-g. We will then compare gas phase and solid phase profiles of discrete and continuous fuel configurations and analyze the different flame spread trend in both configurations

4.1 Characteristics of Concurrent Flame Spread across Discrete Fuel Samples in 0-g

The 1.5-cm gap length is used as a representative case for concurrent flame spread over discrete fuels in microgravity. Figure 4.1 demonstrates time progression of gas temperature and visible flame represented in color map and black contour respectively. Similar to 1-g, discrete case, visible flame contour is defined by heat release rate of $15,000 \text{ kW}/\text{m}^3$. A simulation video that contains different fuel configurations in 0-g is available online.[23] In this configuration, 10 identical fuel samples of 1-cm in length each are separated by 1.5-cm air gap. The forced air flows from the bottom to the top at the

speed of $w_0 = 20 \text{ cm/s}$. The aspect ratio of X to Z is about 1.5 to 1 and therefore, the flame and the flame's distance from the fuel surface is slightly exaggerated.

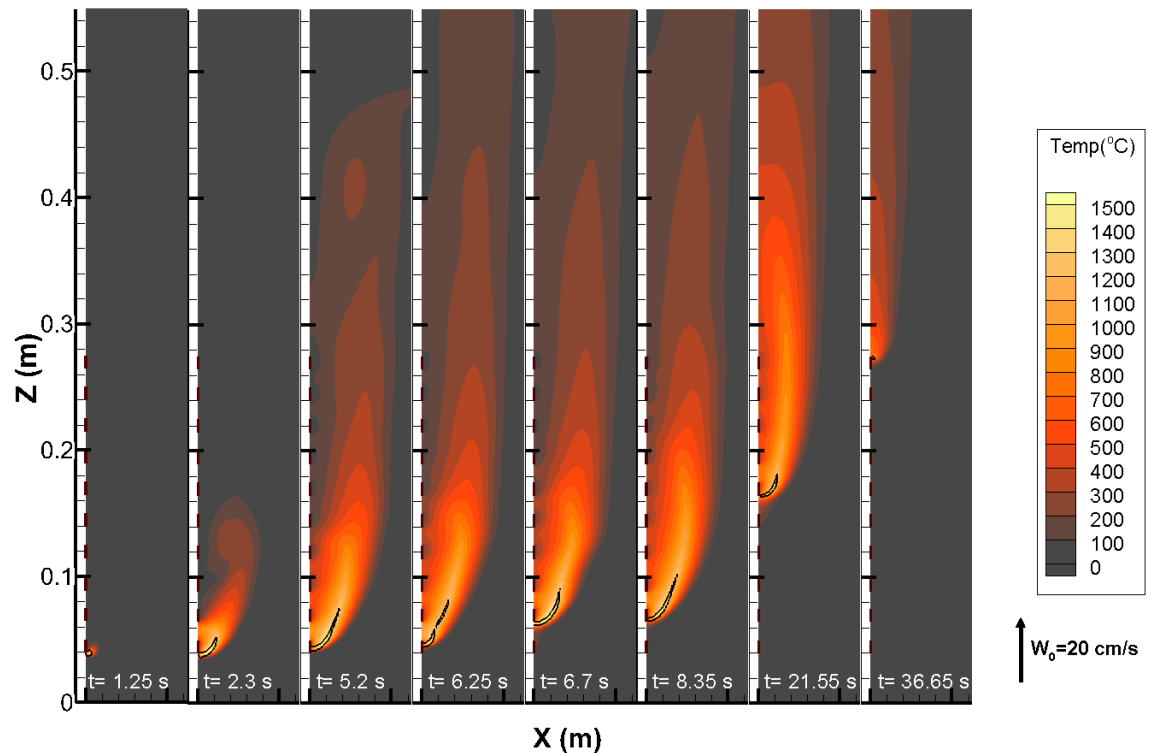
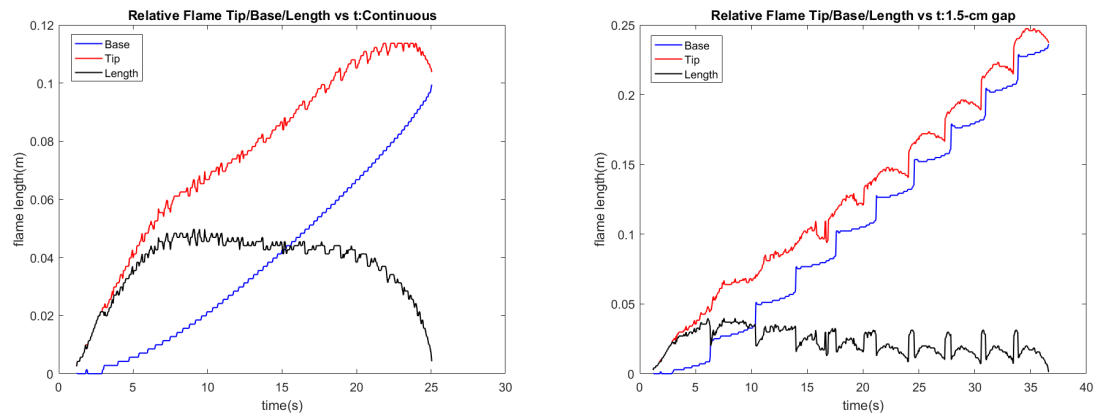


Figure 4.1. Evolution of temperature contours for flame spread across discrete fuel samples. Length of each fuel sample: 1cm. Separation distance: 1.5cm. Black contour: heat release rate = $15,000 \text{ kW/m}^3$.

As shown in the first frame in Fig. cation. Once a flammable gas mixture is achieved, ignition occurs and a diffusion flame is formed. The flame grows very slowly compared to that of 1-g cases. At around $t = 5.2\text{s}$, the flame reaches at about its full length ($\sim 4 \text{ cm}$). At its full length, the flame barely covers 2 fuel blocks, and never gets close to the full fuel span. The flame tip (location of the upper most position of the flame) does not have any unsteady eddies and the flame tip does not fluctuate too much compared to the buoyancy driven flow case. At $t = 6.25 \text{ s}$, the first fuel block (the lowest fuel block)

is almost burned out, while the flame splits into two segments. Then, at $t = 6.7$ s, the flame base "jumps" and completely propagates into the next fuel block. After this initial "jump," the length of the flame reduces slightly and then grows back. This process of split-jump-growth continues until the fuel completely burns out around $t = 37$ s. This is noticeably a slower burning process compared with the 1-g case, where fuel completely burned out in ~ 7 s for 1.5-cm gap discrete configuration.

To show this pattern in detail, flame tip, flame base, and flame length profiles are plotted against time for continuous configuration (Fig. 4.2a) and 1.5-cm gap, discrete configuration (Fig. 4.2b) in Fig. 4.2. In both plots, the red line is the flame tip position (most downstream, flow position), the blue is the flame base position (most upstream position), and the black is the flame length (difference of flame tip and flame base). The flame is tracked in the region where $HRR_{PUV} > 15,000 \text{ kW}/m^3$. Compared to the cases in 1-g, the growth rate of the flame base is steadier and the flame tip position fluctuates less in both configurations. The fluctuation in flame length is within 0.003cm, which is 10% less than the actual flame length. We consider the flame reaches pseudo-steady state for both cases. For continuous fuel, pseudo steady state occurs at $t = 3 - 20$ s, and for discrete fuel case, it happens at $t = 3 - 25$ s. At around $t = 7 - 8$ s, the flame length is at its apex and then decays slowly in the case of continuous configuration in Fig. 4.2a. The discrete case displays similar pattern generally throughout the entire fuel span, as shown in Fig. 4.2b. However, the aforementioned pattern of "split-jump-growth" repeats within each fuel block.



(a) Flame tip, base, and length of a continuous fuel
 (b) Flame tip, base, and length of a 1.5-cm gap fuel configuration

Figure 4.2. Flame location vs time for selected fuel configurations in 0-g

To analyze the effect of the gap length on flame spread rate, the flame base position vs time for different fuel-gap configurations are plotted against time in Fig. 4.3. From the ignition at around $t = 1.25$ s to about $t = 6$ s, the length of the flame grows and the flame base propagates 1-cm, from the point of ignition to the top of the first fuel block. This is identical in all fuel configurations. For continuous configuration, the propagation continues without any interruption and the flame base line is a relatively smooth curve, as shown by the blue line in Fig. 4.3. In discrete fuel, after the first fuel block is completely consumed around $t = 6$ s, the flame base "jumps" to the next fuel block, after each fuel burns out, causing the "steps" observed in Fig. 4.3. In all cases, the flame does not propagate to the next fuel block, until the previous fuel is completely burned out. In other words, the flamelets are not observed in discrete fuel in 0-g simulation. For each individual discrete configuration, the flame base jumps slightly faster as it moves up from one block to another. For instance, in the 1.5-cm discrete fuel configuration (purple line in 4.3), the duration at which the top fuel block burns (about $t = 34 - 36$ s) is much

less than the duration at which the most bottom fuel block burns (about $t = 1.25 - 6s$). In addition, the larger the gap length is, the longer it takes to burn each fuel block after the first segment. Regardless, the flame always travels further at agiven time in configurations with a larger gap size.

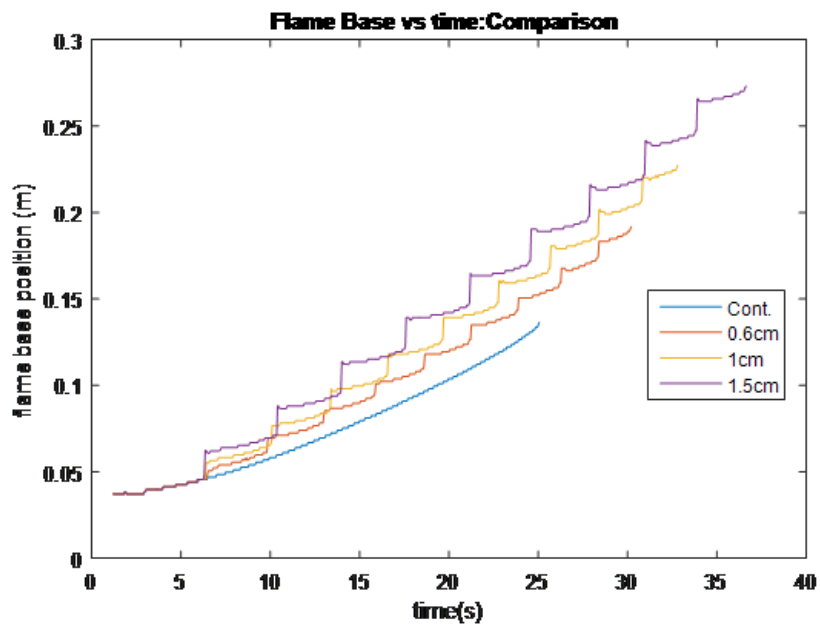


Figure 4.3. Flame base position vs time for different fuel-gap configurations.

4.2 Comparison between Continuous and Discrete Fuel Samples

4.2.1 Pyrolysis and Burning Rate

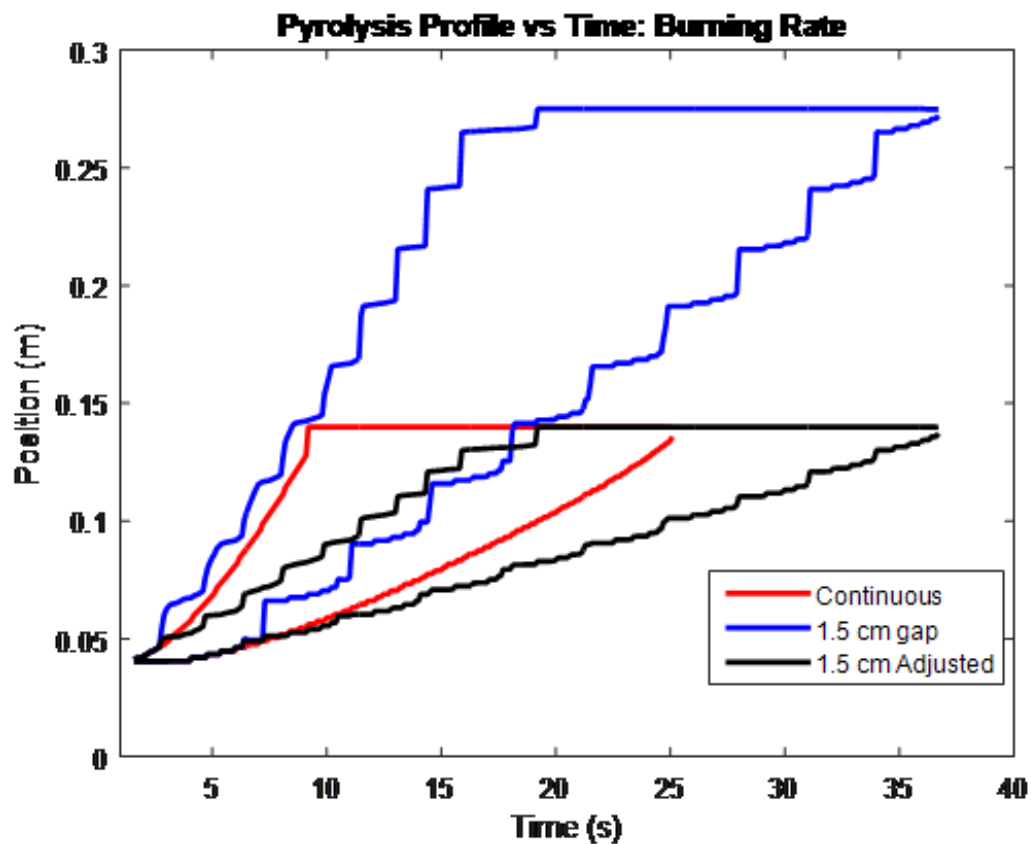


Figure 4.4. Pyrolysis front and base locations vs. time for continuous fuel sample and discrete (gap length = 1.5-cm) fuel samples. The adjusted locations are the locations minus the total length of the gap upstream.

In Fig. 4.4, the location of the pyrolysis regions for the 1.5 cm fuel-percentage discrete fuel configuration is compared with the pyrolysis of the continuous fuel. The pyrolysis regions are defined as the region where the solid burning rate is larger than 0.1 kg/s/m^2 . In Fig. 4.4, the pyrolysis front and base (the most downstream and the

most upstream points of the pyrolysis regions) for the 1.5-cm gap-fuel configuration are shown as blue lines, and those for continuous fuel are shown as red lines. At a given time, the discrete fuel pyrolysis front and base are always ahead of those of the continuous fuel. Similar to 1-g analysis, the adjusted pyrolysis positions (black lines) are also recorded (see “Discrete Adj.” traces) in Fig. 4.4. The adjustment involves subtracting the total length of upstream gap from the unadjusted positions. Unlike 1-g case, however, the entire pyrolysis process of the discrete fuel is slower than the continuous fuel by almost 10 second. This means that, while the flame travels faster due to the presence of physical gaps, it actually burns slower in simulated discrete fuel configuration than continuous fuel.

4.2.2 Gas and Solid Profiles

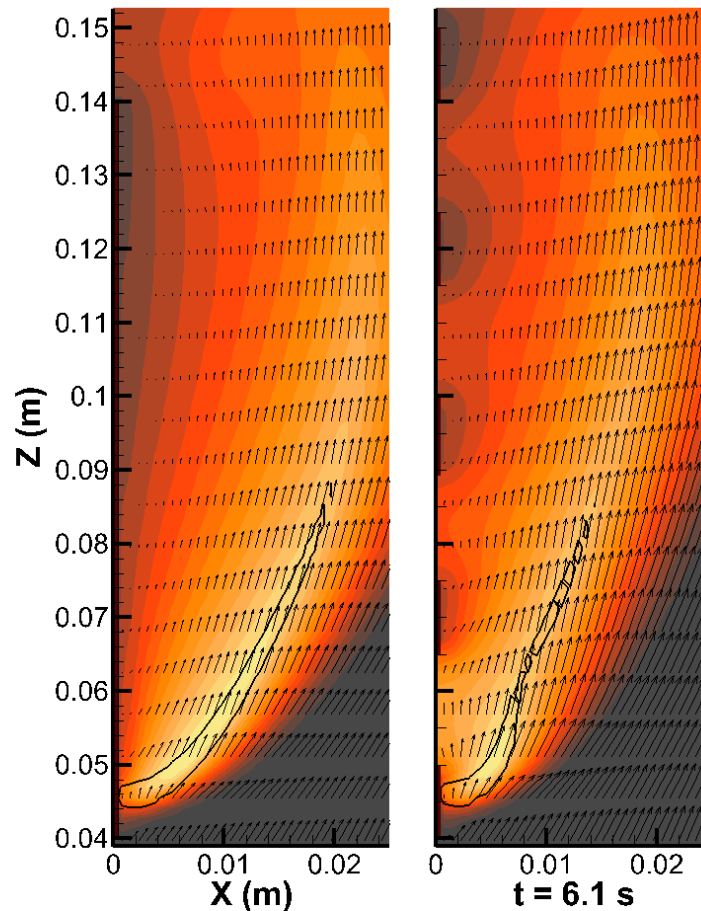


Figure 4.5. Flame shapes (heat release rate = $15,000 \text{ kW/m}^3$), and vector plot for discrete 1.5-cm gap (left) and continuous fuel configurations (right) at $t = 6.1 \text{ s}$.

In Fig. 4.5, the flame shapes and the velocity vector profiles for continuous and discrete configurations (1.5-cm gap) are compared at $t = 6.1 \text{ s}$. Due to the lack of normal velocity coming out from fuel surface in the gap area, the flame stays closer to the fuel surface. As a result, the overall flame standoff distance is shorter in the discrete fuel configuration than that for the continuous fuel. This is similar to the observation from 1-g simulation. The heat flux is greater in the area where the local stand off distance

is smaller (i.e. around the edge of each block). In the Fig. 4.6, some solid phase profiles of discrete (1.5-cm gap) and continuous fuel are compared. The red line is continuous and the blue line represents discrete fuel. In each Fig., the left panel is the heat flux plot, center is the burning rate plot, and the right one is the non-dimensional area density plot. Around the upstream edges of discrete fuels, the local fuel burning rate is higher and are density is lower than continuous fuel. This is caused by the higher heat flux due to smaller local flame stand-off distance. As mentioned earlier, despite the flame traveling faster in discrete fuel, the fuel burns slower as the gap size increases in 0-g. To understand this, we have used a similar approach as in the previous chapter: examine the time evolution of space-integrated solid properties.

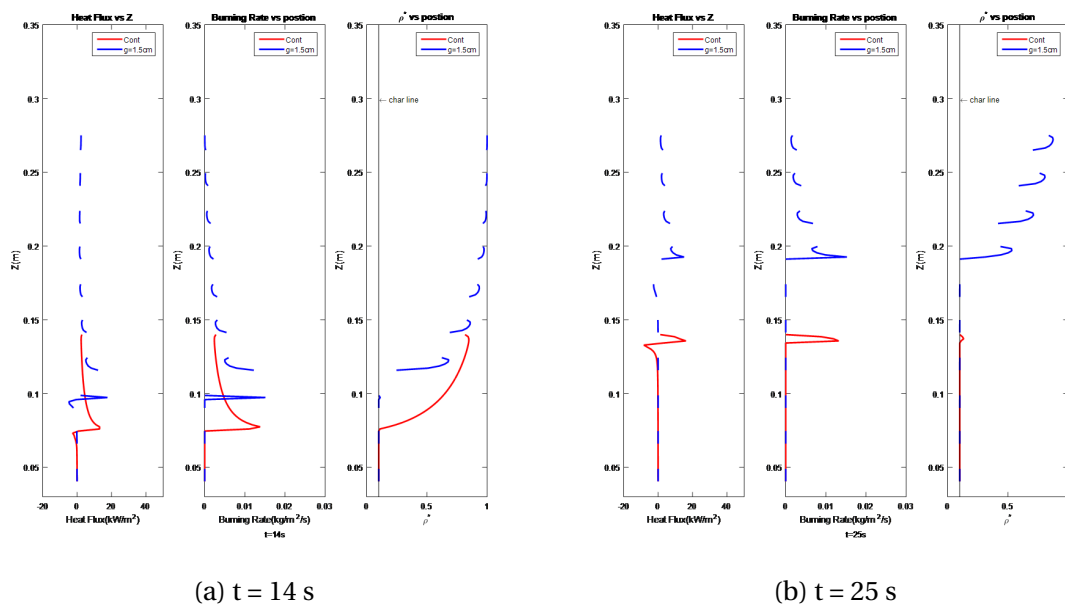
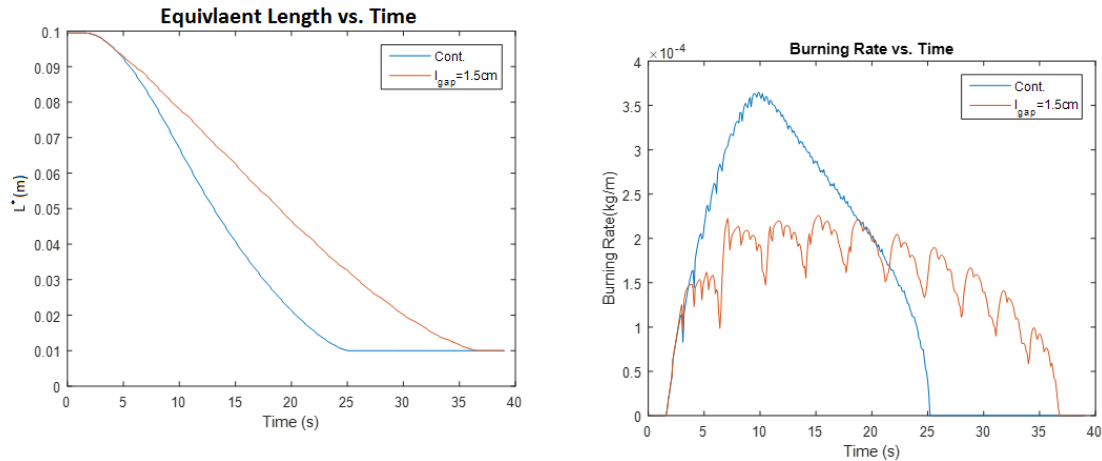
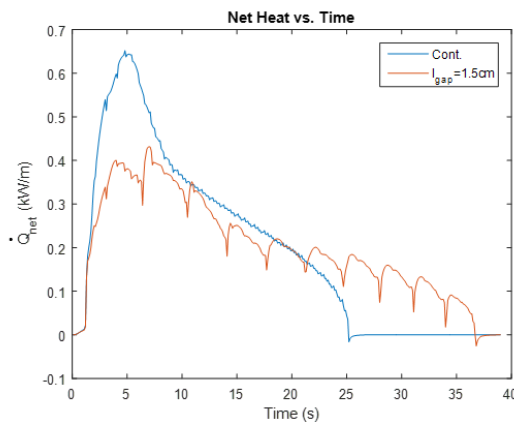


Figure 4.6. Comparison of selected solid phase properties from left to right (Net Heat Flux, Burning Rate, Non-dimensional Area Density) of continuous (red lines) and discrete fuel (blue lines) in 0-g simulations at selected times.

4.3 Net Heat, Burning Rate, and Preheated Length



(a) Equivalent Fuel Length vs time for continu- (b) Burning rate per unit width vs time for con-
 ous and 1.5-cm gap setup tinuous and 1.5-cm gap



(c) Net Heat vs time for continuous and 1.5-cm gap

Figure 4.7. Time evolution of selected solid phase properties of 0-g simulations integrated over virgin fuel length. Blue trace is the continuous configuration and orange line is 1.5-cm gap configuration

Figure 4.7 shows the plot of equivalent length (L^*) vs time (left 4.7a), burning rate per unit width (m'_b) vs time (right 4.7b), and Net Heat on fuel surface (\dot{Q}_{net}) vs time (bottom center 4.7c). The blue line is for the continuous fuel configuration and the orange line is for the discrete fuel configuration. All the L^* , m'_b , and \dot{Q}_{net} values are calculated the

same way as it is explained in equations 3.1 and 3.2. Contrary to the 1-g cases, the slope at which surface density reduces is decreasing much faster for continuous fuel than that of discrete fuel. In addition, the Net Burning Rate per unit length for continuous fuel is greater than discrete fuel over time, until the continuous fuel is close to burnout at $t = 21$ s. Similarly, the Net Heat values for continuous fuel is greater than the discrete fuel from $t = 2$ s to $t = 21$ s, even though some local heat flux values near the edge of each fuel is greater (see Fig.e 4.6).

By closely examining the length of the flame in Fig. 4.2, the flame lengths are quite similar for discrete and continuous fuel, ranging from 4-cm to 4.5-m during the pseudo-steady state. In the continuous case, the entire flame lengths covers the same length of the fuel in continuous case. On the other hand, only two fuel blocks of discrete fuel are covered by the flame (see Fig. 4.5), leaving the effective length at which fuel is covered by the flame (which relates to the pyrolysis length) to only 2-cm at best. One can logically conclude that the covered length will only decrease as the gap length increase, given that the flame length stays similar, which is observed in the simulations. This eventually decreases the preheated length, $l_{preheat}$, and, as a results, decreases \dot{Q}_{net} (see equation 3.3), causing slower burning rate for discrete fuel.

5 Analysis

In the previous chapters the difference between flame spread rate and burning rate between discrete and continuous fuel configurations are examined in both 0-g and 1-g configuration. In this chapter, the different affects of the gap length on the burning rate in 1-g and 0-g will be analyzed. In addition, this chapter will also explain the grid section process for the numerical study.

5.1 Comparison between 1-g and 0-g

The biggest difference between concurrent flame spread in 1-g and 0-g simulation is that in 1-g the flow is driven by a buoyant force and the flow is accelerating in the streamline (upward) direction. On the other hand, 0-g flame spread is driven by external forced air flow in the streamline direction, at a constant, relatively low speed. As shown in Fig. 5.1, the magnitude of the velocity vector inside the reaction zone in 1-g (the left panel in the Fig.) is much larger than the velocity magnitude in 0-g. Another noticeable traits are that the flame stand-off distance in 0-g is much larger, compared to 1-g, and that the flame length is much longer in 1-g than in 0-g. Combined together, they produce multiple outcomes.

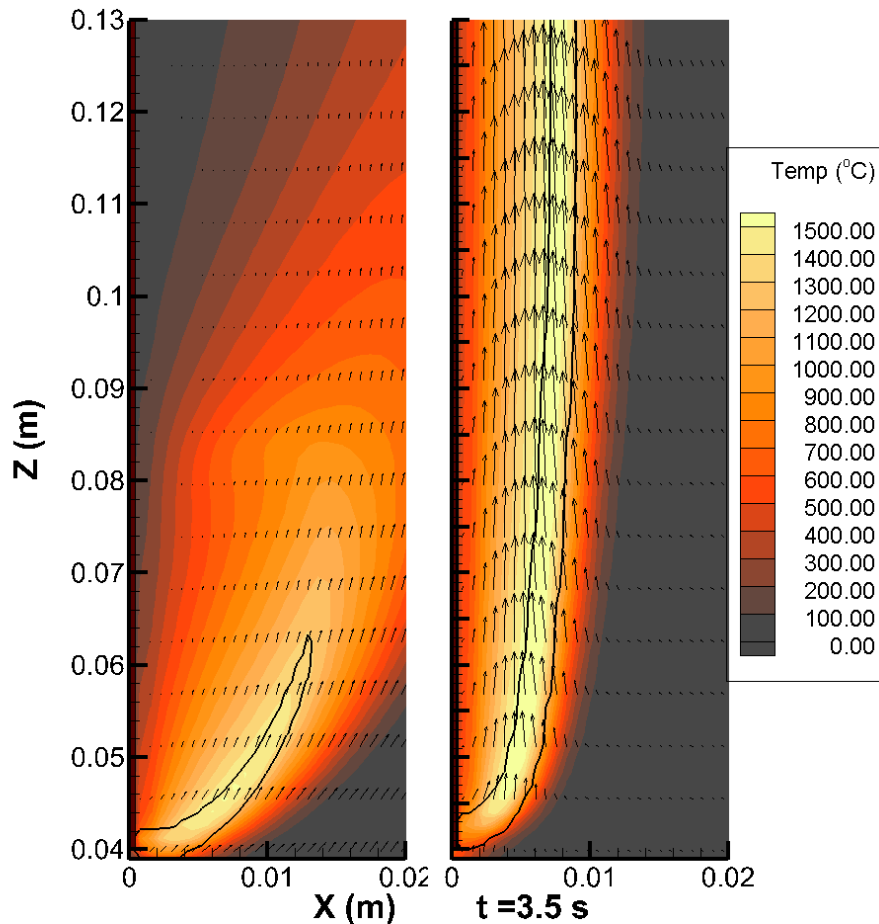


Figure 5.1. A side-by-side comparison between the flame profile and vector plot in 0-g (left) and 1-g (right)

In Fig. 5.2, some solid phase properties and gas phase flame profile of continuous fuel in 0-g (left in 5.2a) and 1-g (right 5.2b) is plotted around the time when the flame base is at about $z = 0.06$ m. On the left panel of each Fig., z axis (streamline direction) value is plotted against the heat flux, where the blue line represents the radiative heat flux, red represents convective heat flux, and thin dark line represents the net heat flux. In the middle panel of each Fig., the flame profile is plotted and the right plane contains the non-dimensionalised area density (ρ^*) plot. The flow speed in 0-g results in lower convective heat flux. The Heat Flux vs z - position diagram shows that the local

maximum value of convective heat flux(both occurring at about $z = 0.06$ m) is about 50 kW/m^2 less for 0-g than 1-g. In addition, the reduced flame length exposes less fuel in downstream direction to the flame in 0-g flow. This is shown by the area density vs position plot. In 0-g area density plot in 5.2a, the ρ^* value increases and gets close to $\rho^* = 1$, whereas ρ^* plot in 1-g does not get close to 1. In other words, the longer flame length pyrolyzed more fuel in the downstream direction.

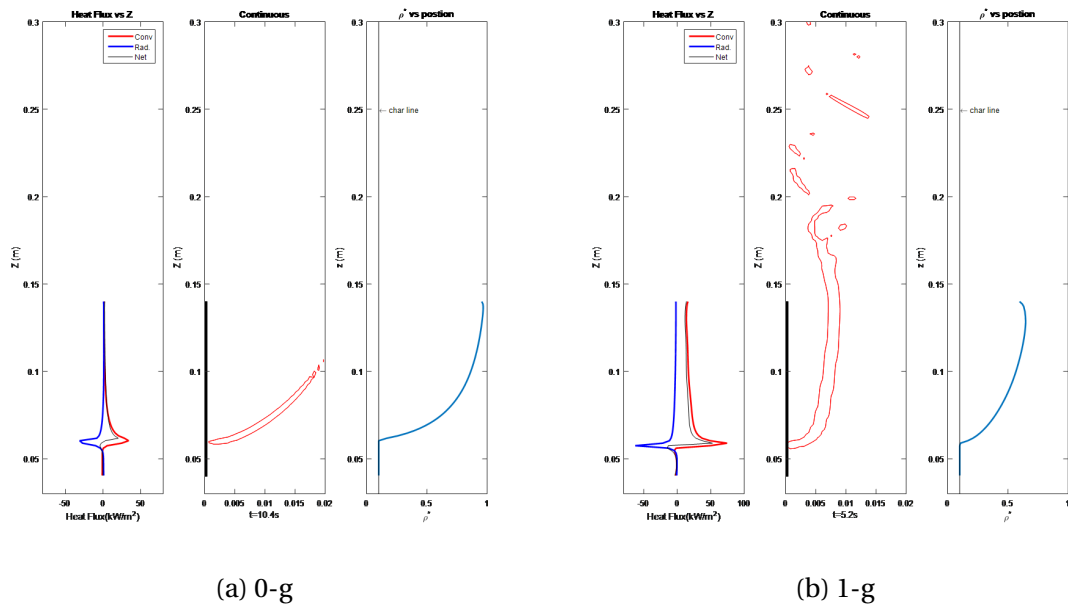


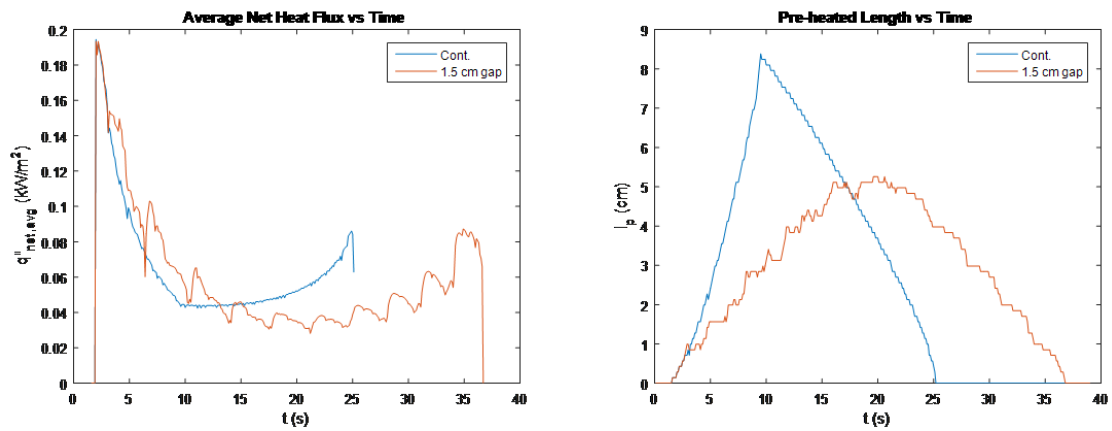
Figure 5.2. Comparison of different modes of heat flux, flame profile, and surface density at selected instances

The same effect happens in discrete fuel configuration. However, since the flame length at pseudo-steady state in 0-g does not fully cover the total fuel span, the pre-heated length of discrete fuel is much smaller than that of continuous fuel. In order to determine how much heat flux is introduced to an unburned fuel, the Net Heat, \dot{Q}_{net} , is normalized by the un-burned fuel length, l_p . Introducing a new parameter $\dot{q}''_{net,unburned}$, where

$$\dot{q}_{net,unburned}'' = \frac{1}{l_p} \int_{l_p} \dot{q}_{net}'' dz \quad (5.1)$$

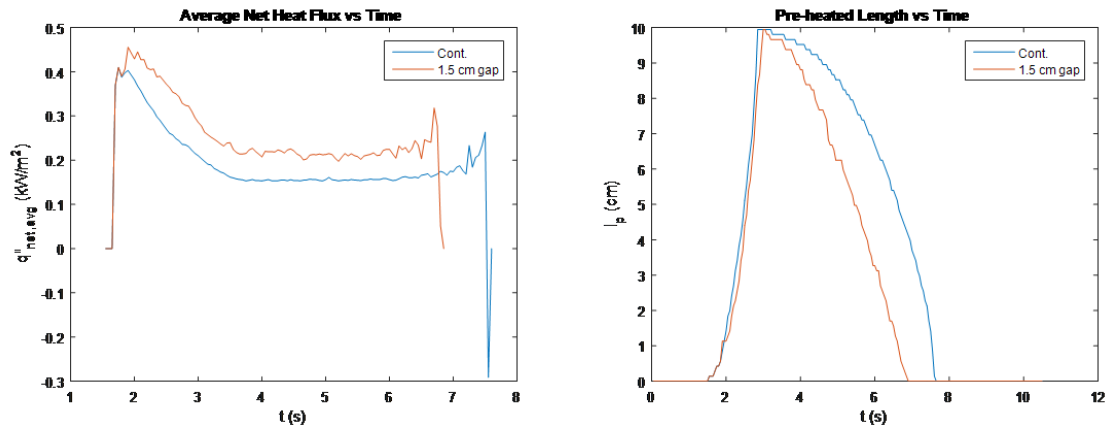
Figure 5.3 contains both $\dot{q}_{net,unburned}''$ vs time plot and $l_{preheat}$ vs time plot in both 0-g (Fig. 5.3a and 5.3b) and 1-g (Fig. 5.3c and 5.3d). Blue line represents continuous and red line represents 1.5-cm gap discrete configuration. Consistent with what is discovered from the previous chapter, the unburned portion of discrete fuel tend to experience higher total net heat. In 0-g case, the net heat per unburned fuel values for discrete fuel is not significantly greater than that of continuous as shown in Fig. 5.3a. However, since less fuel is covered by the flame, the preheated length, $l_{preheat}$, for continuous fuel is much greater than the discrete fuel, as shown by the blue line in Fig. 5.3b.

Burning rate is dictated by the net heat value \dot{Q}_{net} . As explained in section 3.4, \dot{Q}' is closely related to \bar{q}'' and $l_{preheat}$. If either increases, while the other remains similar, \dot{Q}' increases. In 1-g, the burning rate discrepancy among the gap lengths is caused by \dot{q}'' , whereas in 0-g, it is mostly caused by $l_{preheat}$. In other words, the opposite burning rate trend from 1-g to 0-g (where discrete fuel configuration with larger gaps burns slower in 0-g unlike in 1-g) is caused by the decreasing $l_{preheat}$.



(a) Average Net Heat Flux vs Time in 0-g simulation

(b) Preheat length vs Time in 0-g simulation



(c) Average Net Heat Flux vs Time in 1-g simulation

(d) Preheat length vs Time in 1-g simulation

Figure 5.3. Selected solid phase properties of 0-g and 1-g simulations integrated over unburned fuel length. Blue trace is the continuous configuration and orange line is 1.5-cm gap configuration

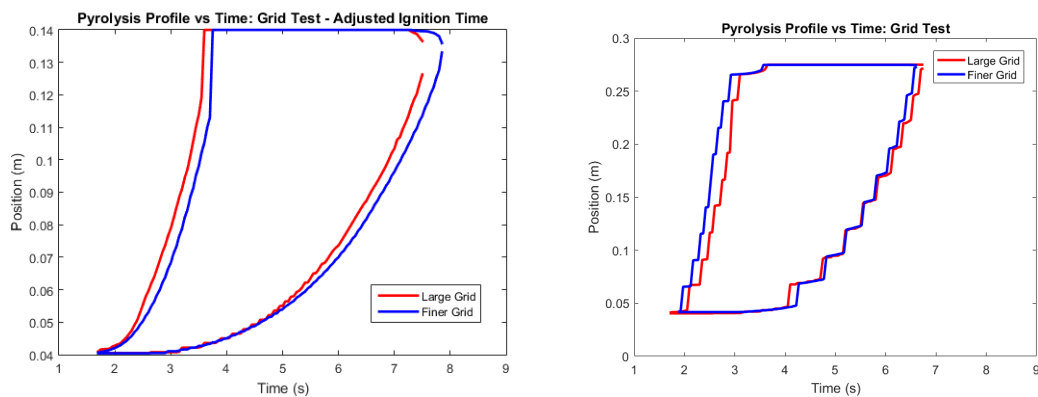
5.2 Grid Setup

In order to capture micro-scale of turbulent flow, DNS typically requires extremely fine grid sizes, which results in substantial increase of computing time. Fortunately, this study is mainly interested in propagation of flame over discrete fuel, especially the flame

base. In other words, the simulation does not have to capture the details of unsteady eddies that occur at the tip of buoyancy driven flame or the edge of reaction zone in the flame. Furthermore, since this model simulates a very thin fuel of a single grid size thickness, the grid does not have to be fine enough to resolve small eddies generated due to fluid dynamic edge effect. Regardless, it is important to find the optimum grid size at which it is small enough there is no significant difference in flame propagation but not enough to compromise computational expense by a significant factor.

In order to simulate "paper thin" fuel thickness, it is determined the minimum size of the x-axis grid, δ_x , has to be greater than the half the obstruction thickness, τ_f , which was modeled after the actual fuel thickness. This is to ensure that the fuel thickness of the fuel does not exceed a single grid size:

$$\frac{\delta x}{\tau_f} > \frac{1}{2} \quad ; \quad \tau_f = 0.3937 \text{ mm}$$



(a) Continuous Fuel Configuration Grid Dependency Check in 1-g: Pyrolysis Profile (b) 1.5-cm gap Fuel-Gap Configuration Grid Dependency Check in 1-g: Pyrolysis Profile

Figure 5.4. Grid Dependency Study on different configurations. The blue lines are finer grid simulation and the red lines are regular, coarse grid result.

Table 5.1. Number of grid used in Fine Grid and Coarse Grid simulation. The resulting grid dimensions are listed on the bottom two rows.

	Large Grid	Finer Grid
n_x	66	132
n_z	387	1000
n_{total}	25,542	132,000
δ_x (mm)	0.76	0.38
δ_z (mm)	1.42	0.55

The Fig. 5.4 shows the result of grid dependency analysis for both continuous (Fig. 5.4a) and discrete fuel configuration, 1.5-cm gap in particular (Fig. 5.4b). The pyrolysis profiles are plotted from fine grid and coarse grid simulations. The red lines are coarse grid results, while the blue lines are fine grid results. Table 5.1 shows the number of grids used in x domain, z domain and the resulting grid size. By comparing the results from Fig. 5.4 qualitatively, the grid size does not affect the overall trend where the pyrolysis spread rate increases as the gap size increase in 1-g simulation. For a quantitative grid analysis, an average pyrolysis spread rate is defined such that:

$$v_{p,avg} = \frac{\text{Pyrolysis length}}{\text{Time to reach pyrolysis length}} = \frac{z_{pyro2} - z_{pyro1}}{t_2 - t_1}$$

where the pyrolysis length is obtained by subtracting pyrolysis position at $t = t_1$ (z_{pyro1}) from the pyrolysis position at $t = t_2$ (z_{pyro2}). The average pyrolysis front spread rate ($v_{pf,avg}$) and the average pyrolysis base spread rate ($v_{pb,avg}$) are calculated for both fine grid and coarse grid. The result is tabulated in table 5.2 For continuous configuration, the biggest margin of error is 7.49%, occurring at the average pyrolysis front spread rate. For continuous configuration, the biggest margin of error is 12.3%, also occurring

at the average pyrolysis front spread rate. However, the run time for finer grid takes almost about 3 weeks per simulation, while the coarse grid takes about 6 days per simulation. The margin of error is not significant enough to change the overall trend in burning rate, which is the main purpose of this study. In other words, if the grid is fine enough to capture the trend in discrete fuel burning, it is not worth pursuing further accuracy in exchange for computational time.

Table 5.2. Qualitative grid analysis comparing average pyrolysis spread rate at different grid resolution

<u>Continuous configuration</u>			
	Fine Grid	Coarse Grid	ϵ_s (%)
$v_{pf,avg}(m/s)$	0.048488	0.052121	7.493
$v_{pb,avg}(m/s)$	0.015052	0.014776	1.834
<u>Discrete Fuel with 1.5-cm gap</u>			
	Fine Grid	Coarse Grid	ϵ_s (%)
$v_{pf,avg}(m/s)$	0.136829	0.119995	12.303
$v_{pb,avg}(m/s)$	0.045672	0.045743	0.1547

6 Conclusions

In this study, concurrent flame spread over thin solid fuels is numerically examined in discrete and continuous fuel configurations, using Fire Dynamic Simulator. The simulation is performed under two different types of flow: a buoyancy driven flow in 1-g and a forced convective flow in 0-g where the flow velocity of $w_0 = 20\text{cm/s}$ is prescribed. Two-dimensional Direct Numerical Simulations (DNS) is performed, including one-step finite-rate gas-phase combustion, one-step first-order solid Arrhenius pyrolysis, and gray gas radiation modeling for all gas species. First, we examined the time evolution of flame spread over different configurations. Then we examined both solid phase and gas phase properties. Solid phase properties are used to construct pyrolysis profiles and the gas phase properties are used to track the location of the flame base. The key findings are:

- 1) The flame spread rate is always affected by the presence of the gap in both 1-g and 0-g. Due to the presence of the gap, the flame always travels faster in discrete fuel than in continuous fuel. This is consistent in both 0-g cases and 1-g cases. However, the flame spreads much faster (almost ~ 5 times) in 1-g buoyancy driven flow than in the forced concurrent flow in 0-g at $w_0 = 20\text{cm/s}$

2) The burning rate of the fuel is determined by the total heat value, \dot{Q}_{net} . This value is dependent on two parameters; a pre-heated length, $l_{preheat}$, and local heat flux from the flame to the fuel surface, \dot{q}'' . If one parameter increases, when the other stays similar, \dot{Q}_{net} increases.

3) In both 1-g and 0-g, the flame standoff distance decreases at the gaps, resulting in a reduced stand-off distance. The smaller stand-off distance causes increased heat flux to the fuel. This causes higher local heat flux values in discrete fuel, when compared to the local heat flux values in continuous fuel.

4) In 1-g, a fully grown flame exceeds the total fuel span in all configurations, and the preheated lengths are similar in all configurations (i.e. total fuel length). However, the increased local heat flux in discrete fuel causes greater \dot{Q}_{net} values. As a result, the fuel burns faster for discrete fuel compared to continuous fuel. As the gap increases, the burning rate increases in 1-g.

5) In 0-g at $w_0 = 20\text{ cm/s}$, the flame length is much smaller than the smallest possible total fuel span (10-cm). As a result, the flame "covers" less effective fuel length and $l_{preheat}$ decreases as the gap increases. Since the local heat flux value is not significantly different in each configuration, \dot{Q}_{net} are more affected by $l_{preheat}$. Therefore, in 0-g the fuel burns slower as the gap increases.

As for the potential future study, additional fuel-gap configurations can be examined. For instance, this model was only limited to 1-cm fuel length. However, a different fuel lengths such as 3-cm, or 5-cm, or even at a larger scale study can be conducted at many different possible fuel-gap permutations. With different fuel length, it can also be examined if similar fuel-gap ratios (i.e. 1-cm fuel to 0.5-cm gap and 5-cm fuel to 2.5-cm gap) display similar flame spread patterns.

The effect of the boundary layer can also be examined. Instead of using gaps, an inert, adiabatic material with the same thickness as the filter paper can be inserted in between fuels, instead of air gap. In addition, the effect of kinetics on the spread rate and the accuracy of the simulation can also be evaluated.

Appendix A

FDS Input Codes

This section contains the some selected FDS input code

1 1-g Input Code

Continuous Configuration

```
f1g0fp100.fds: 1cm fuel continuous run
-Symmetry plane is kept
-fuel block length 1 cm
-Separation distance: 0 cm (fuel 1cm/ air 0 cm,
resulting in fuel percentage of 100%)
-total of 10 fuel blocks
-Total Runtime 15s
-Oxygen Mass Fraction as Output
-Different Name convention (f1=> fuel length, g0=>
gap length, fp100=> fuel percentage)

&HEAD CHID='Discrete Run40', TITLE='Symmetric
Cardboard Setup' /
```



```

SPEC_ID_NU      = 'CELLULOSE ', 'OXYGEN ', 'WATER VAPOR
', 'CARBON DIOXIDE '
NU(1:4)        = -1, -6, 5, 6
SPEC_ID_N_S    = 'CELLULOSE ', 'OXYGEN '
N_S(1:2)       = 1, 1
HEAT_OF_COMBUSTION    = 15800.
HRRPUA_SHEET        = 1.0E10 /

&MATL ID                = 'CARDBOARDMEDIUM '
EMISSIVITY              = 1.0
SPECIFIC_HEAT           = 1.20
CONDUCTIVITY            = 0.06
DENSITY                 = 555.3

N_REACTIONS             = 1
A(1)                    = 1.00E10
E(1)                    = 1.25E5
N_S(1)                  = 1.
SPEC_ID(1:4,1)          = 'CELLULOSE ', 'OXYGEN ', '
WATER VAPOR ', 'CARBON DIOXIDE '
NU_SPEC(1:4,1)         = 0.9,0,0,0
NU_MATL(1,1)           = 0.1
MATL_ID                 = 'CHARMEDIUM '

```

HEAT_OF_REACTION = 752.8
HEAT_OF_COMBUSTION = 15800. /

&MATL ID = 'CARDBOARDLINER'
EMISSIVITY = 1.0
SPECIFIC_HEAT = 1.20
CONDUCTIVITY = 0.06
DENSITY = 504.6 /

&MATL ID = 'CHARMEDIUM'
EMISSIVITY = 1.0
SPECIFIC_HEAT = 1.20
CONDUCTIVITY = 0.06
DENSITY = 555.3 /

&MATL ID = 'STEEL'
FYI = '310 stainless at 320K'
EMISSIVITY = 1.0
SPECIFIC_HEAT = 0.48
CONDUCTIVITY = 13.2

```
DENSITY                = 7870. /

&SURF ID                = 'MEDIUM'
COLOR                   = 'SIENNA'
MATL_ID                 = 'CARDBOARDMEDIUM'
THICKNESS               = 0.000115
LAYER_DIVIDE           = 1.0
NO_SLIP                 = .TRUE.
BACKING                 = 'INSULATED' /

&SURF ID                = 'MEDIUMINERT'
COLOR                   = 'SIENNA'
MATL_ID                 = 'CARDBOARDMEDIUM'
THICKNESS               = 0.000165
LAYER_DIVIDE           = 0.0
NO_SLIP                 = .TRUE. /

&SURF ID                = 'LINER'
COLOR                   = 'SIENNA'
MATL_ID                 = 'CARDBOARDLINER'
THICKNESS               = 0.00041
CELL_SIZE_FACTOR       = 1000.
```

```
NO_SLIP                = .TRUE. /

&SURF ID                = 'TABLE'
COLOR                   = 'GRAY'
MATL_ID                 = 'STEEL'
THICKNESS               = 0.05
CELL_SIZE_FACTOR       = 1000.
NO_SLIP                = .TRUE. /

&SURF ID                = 'PILOT'
COLOR                   = 'BLACK'

&OBST XB=0.0,0.0003937,0.0,0.05,0.04,0.05
SURF_ID6='MEDIUMINERT','MEDIUM','MEDIUMINERT',
MEDIUMINERT','MEDIUMINERT','MEDIUMINERT' /

&OBST XB=0.0,0.0003937,0.0,0.05,0.05,0.06
SURF_ID6='MEDIUMINERT','MEDIUM','MEDIUMINERT',
MEDIUMINERT','MEDIUMINERT','MEDIUMINERT' /

&OBST XB=0.0,0.0003937,0.0,0.05,0.06,0.07
```

```
SURF_ID6='MEDIUMINERT','MEDIUM','MEDIUMINERT','  
MEDIUMINERT','MEDIUMINERT','MEDIUMINERT' /
```

```
&OBST XB=0.0,0.0003937,0.0,0.05,0.07,0.08
```

```
SURF_ID6='MEDIUMINERT','MEDIUM','MEDIUMINERT','  
MEDIUMINERT','MEDIUMINERT','MEDIUMINERT' /
```

```
&OBST XB=0.0,0.0003937,0.0,0.05,0.08,0.09
```

```
SURF_ID6='MEDIUMINERT','MEDIUM','MEDIUMINERT','  
MEDIUMINERT','MEDIUMINERT','MEDIUMINERT' /
```

```
&OBST XB=0.0,0.0003937,0.0,0.05,0.09,0.10
```

```
SURF_ID6='MEDIUMINERT','MEDIUM','MEDIUMINERT','  
MEDIUMINERT','MEDIUMINERT','MEDIUMINERT' /
```

```
&OBST XB=0.0,0.0003937,0.0,0.05,0.10,0.11
```

```
SURF_ID6='MEDIUMINERT','MEDIUM','MEDIUMINERT','  
MEDIUMINERT','MEDIUMINERT','MEDIUMINERT' /
```

```
&OBST XB=0.0,0.0003937,0.0,0.05,0.11,0.12
```

```
SURF_ID6='MEDIUMINERT','MEDIUM','MEDIUMINERT','  
MEDIUMINERT','MEDIUMINERT','MEDIUMINERT' /
```

```
&OBST XB=0.0,0.0003937,0.0,0.05,0.12,0.13
SURF_ID6='MEDIUMINERT','MEDIUM','MEDIUMINERT','
MEDIUMINERT','MEDIUMINERT','MEDIUMINERT' /

&OBST XB=0.0,0.0003937,0.0,0.05,0.13,0.14
SURF_ID6='MEDIUMINERT','MEDIUM','MEDIUMINERT','
MEDIUMINERT','MEDIUMINERT','MEDIUMINERT' /

&VENT MB='XMIN', SURF_ID='MIRROR' /
&VENT MB='XMAX', SURF_ID='OPEN' /
&VENT MB='ZMAX', SURF_ID='OPEN' /
&VENT MB='ZMIN', SURF_ID='TABLE' /

&OBST XB=0.0,0.001,0.0,0.05,0.038,0.039, SURF_ID='
HOT', DEVC_ID='TIMER1' /
&SURF ID='HOT',NO_SLIP=.TRUE.,TMP_FRONT=1000./
&DEVC ID='TIMER1',XYZ=0.0045,0.00191,0.4, SETPOINT
=5,QUANTITY='TIME',INITIAL_STATE=.TRUE./

&SLCF PBX=0.05, QUANTITY='TEMPERATURE', VECTOR=.
TRUE. /
&SLCF PBZ=0.05, QUANTITY='TEMPERATURE', VECTOR=.
TRUE. /
```

```
&SLCF PBZ=0.082, QUANTITY='TEMPERATURE', VECTOR=.  
TRUE. /
```

```
&SLCF PBZ=0.114, QUANTITY='TEMPERATURE', VECTOR=.  
TRUE. /
```

```
&SLCF PBZ=0.152, QUANTITY='TEMPERATURE', VECTOR=.  
TRUE. /
```

```
&SLCF PBZ=0.168, QUANTITY='TEMPERATURE', VECTOR=.  
TRUE. /
```

```
&SLCF PBZ=0.184, QUANTITY='TEMPERATURE', VECTOR=.  
TRUE. /
```

```
&SLCF PBZ=0.05, QUANTITY='PRESSURE' /
```

```
&SLCF PBZ=0.082, QUANTITY='PRESSURE' /
```

```
&SLCF PBZ=0.114, QUANTITY='PRESSURE' /
```

```
&SLCF PBZ=0.152, QUANTITY='PRESSURE' /
```

```
&SLCF PBZ=0.168, QUANTITY='PRESSURE' /
```

```
&SLCF PBZ=0.05, QUANTITY='HRRPUV', VECTOR=.TRUE. /
```

```
&SLCF PBZ=0.05, QUANTITY='HRRPUV', VECTOR=.TRUE. /
```

```
&SLCF PBZ=0.082, QUANTITY='HRRPUV', VECTOR=.TRUE.
```

```
/
```

```
&SLCF PBZ=0.114, QUANTITY='HRRPUV', VECTOR=.TRUE.
```

```
/
```

```
&SLCF PBZ=0.152, QUANTITY='HRRPUV', VECTOR=.TRUE.
/
&SLCF PBZ=0.168, QUANTITY='HRRPUV', VECTOR=.TRUE.
/
&SLCF PBZ=0.184, QUANTITY='HRRPUV', VECTOR=.TRUE.
/

&SLCF PBZ=0.05, QUANTITY='MASS FRACTION', SPEC_ID =
'OXYGEN', VECTOR=.TRUE./
&SLCF PBZ=0.05, QUANTITY='MASS FRACTION', SPEC_ID =
'OXYGEN', VECTOR=.TRUE./
&SLCF PBZ=0.082, QUANTITY='MASS FRACTION', SPEC_ID
= 'OXYGEN', VECTOR=.TRUE./
&SLCF PBZ=0.114, QUANTITY='MASS FRACTION', SPEC_ID
= 'OXYGEN', VECTOR=.TRUE./
&SLCF PBZ=0.152, QUANTITY='MASS FRACTION', SPEC_ID
= 'OXYGEN', VECTOR=.TRUE./
&SLCF PBZ=0.168, QUANTITY='MASS FRACTION', SPEC_ID
= 'OXYGEN', VECTOR=.TRUE./
&SLCF PBZ=0.184, QUANTITY='MASS FRACTION', SPEC_ID
= 'OXYGEN', VECTOR=.TRUE./
```



```
&SLCF PBZ=0.152, QUANTITY='MASS FRACTION',SPEC_ID  
= 'WATER VAPOR', VECTOR=.TRUE./
```

```
&SLCF PBZ=0.168, QUANTITY='MASS FRACTION',SPEC_ID  
= 'WATER VAPOR', VECTOR=.TRUE./
```

```
&SLCF PBZ=0.184, QUANTITY='MASS FRACTION',SPEC_ID  
= 'WATER VAPOR', VECTOR=.TRUE./
```

```
&SLCF PBY=0.05, QUANTITY='MASS FRACTION',SPEC_ID =  
'CARBON DIOXIDE', VECTOR=.TRUE./
```

```
&SLCF PBZ=0.05, QUANTITY='MASS FRACTION',SPEC_ID =  
'CARBON DIOXIDE', VECTOR=.TRUE./
```

```
&SLCF PBZ=0.082, QUANTITY='MASS FRACTION',SPEC_ID  
= 'CARBON DIOXIDE', VECTOR=.TRUE./
```

```
&SLCF PBZ=0.114, QUANTITY='MASS FRACTION',SPEC_ID  
= 'CARBON DIOXIDE', VECTOR=.TRUE./
```

```
&SLCF PBZ=0.152, QUANTITY='MASS FRACTION',SPEC_ID  
= 'CARBON DIOXIDE', VECTOR=.TRUE./
```

```
&SLCF PBZ=0.168, QUANTITY='MASS FRACTION',SPEC_ID  
= 'CARBON DIOXIDE', VECTOR=.TRUE./
```

```
&SLCF PBZ=0.184, QUANTITY='MASS FRACTION',SPEC_ID  
= 'CARBON DIOXIDE', VECTOR=.TRUE./
```

```
&BNDF QUANTITY='WALL TEMPERATURE', CELL_CENTERED=.
TRUE. /

&BNDF QUANTITY='NET HEAT FLUX', CELL_CENTERED=.
TRUE. /

&BNDF QUANTITY='INCIDENT HEAT FLUX', CELL_CENTERED
=.TRUE. /

&BNDF QUANTITY='BURNING RATE', CELL_CENTERED=.TRUE
. /

&BNDF QUANTITY='SURFACE DENSITY', CELL_CENTERED=.
TRUE. /

&BNDF QUANTITY='CONVECTIVE HEAT FLUX',
CELL_CENTERED=.TRUE. /

&BNDF QUANTITY='RADIATIVE HEAT FLUX',
CELL_CENTERED=.TRUE. /

&DUMP DT_PL3D=0.05, PLOT3D_QUANTITY(1:5)='
TEMPERATURE', 'HRRPUV', 'U-VELOCITY', 'W-VELOCITY', 'MASS
FRACTION',
PLOT3D_SPEC_ID(5)='OXYGEN', WRITE_XYZ=.TRUE./

&TAIL /
```

```
fig0fp100.fds: 1cm fuel continuous run
-Symmetry plane is kept
-fuel block length 1 cm
-Separation distance: 1 cm (fuel 1cm/ air 1 cm, resulting
  in fuel percentage of 50%)
-total of 10 fuel blocks
-Total Runtime 15s
-Oxygen Mass Fraction as Output
-Different Name convention (f1=> fuel length, g0=> gap
  length, fp100=> fuel percentage)

&HEAD CHID='Discrete Run41', TITLE='Symmetric Cardboard
  Setup' /

&MESH ID='cardboard', IJK=66,1,387, XB
  =0.0,0.05,0.0,0.05,0.0,0.55/

&TIME T_END=12.0, WALL_INCREMENT=1 /

&DUMP DT_RESTART=1.0, NFRAMES=1100 /

&MISC BAROCLINIC=.FALSE., NOISE=.FALSE., DNS=.TRUE./
```

```
&RADI RADIATIVE_FRACTION=0. /

&SPEC ID='NITROGEN', BACKGROUND=.TRUE./
&SPEC ID = 'CELLULOSE', FORMULA = C6H10O5, MW=162.0/
&SPEC ID = 'OXYGEN', MASS_FRACTION_0 = 0.23/
&SPEC ID = 'WATER VAPOR' /
&SPEC ID = 'CARBON DIOXIDE' /

&REAC FUEL          = 'CELLULOSE'

A          = 4.23E14
E          = 1.13E5
SPEC_ID_NU    = 'CELLULOSE', 'OXYGEN', 'WATER VAPOR', '
              CARBON DIOXIDE'
NU(1:4)      = -1, -6, 5, 6
SPEC_ID_N_S   = 'CELLULOSE', 'OXYGEN'
N_S(1:2)     = 1, 1
HEAT_OF_COMBUSTION = 15800.
HRRPUA_SHEET  = 1.0E10 /

&MATL ID          = 'CARDBOARDMEDIUM'
EMISSIVITY        = 1.0
SPECIFIC_HEAT     = 1.20
```

```
CONDUCTIVITY          = 0.06
DENSITY                = 555.3

N_REACTIONS           = 1
A(1)                  = 1.00E10
E(1)                  = 1.25E5
N_S(1)                = 1.
SPEC_ID(1:4,1)       = 'CELLULOSE', 'OXYGEN', 'WATER VAPOR
    ', 'CARBON DIOXIDE'
NU_SPEC(1:4,1)       = 0.9,0,0,0
NU_MATL(1,1)         = 0.1
MATL_ID               = 'CHARMEDIUM'
HEAT_OF_REACTION     = 752.8
HEAT_OF_COMBUSTION   = 15800. /

&MATL ID              = 'CARDBOARDLINER'
EMISSIVITY            = 1.0
SPECIFIC_HEAT        = 1.20
CONDUCTIVITY          = 0.06
DENSITY               = 504.6 /
```

```
&MATL ID                = 'CHARMEDIUM'  
EMISSION                = 1.0  
SPECIFIC_HEAT           = 1.20  
CONDUCTIVITY            = 0.06  
DENSITY                  = 555.3 /
```

```
&MATL ID                = 'STEEL'  
FYI                     = '310 stainless at 320K'  
EMISSION                = 1.0  
SPECIFIC_HEAT           = 0.48  
CONDUCTIVITY            = 13.2  
DENSITY                  = 7870. /
```

```
&SURF ID                = 'MEDIUM'  
COLOR                   = 'SIENNA'  
MATL_ID                 = 'CARDBOARDMEDIUM'  
THICKNESS               = 0.000115  
LAYER_DIVIDE            = 1.0  
NO_SLIP                 = .TRUE.  
BACKING                  = 'INSULATED' /
```

```
&SURF ID                = 'MEDIUMINERT'
```

```
COLOR                = 'SIENNA '  
MATL_ID              = 'CARDBOARDMEDIUM '  
THICKNESS            = 0.000165  
LAYER_DIVIDE         = 0.0  
NO_SLIP              = .TRUE. /  
  
&SURF ID              = 'LINER '  
COLOR                = 'SIENNA '  
MATL_ID              = 'CARDBOARDLINER '  
THICKNESS            = 0.00041  
CELL_SIZE_FACTOR     = 1000.  
NO_SLIP              = .TRUE. /  
  
&SURF ID              = 'TABLE '  
COLOR                = 'GRAY '  
MATL_ID              = 'STEEL '  
THICKNESS            = 0.05  
CELL_SIZE_FACTOR     = 1000.  
NO_SLIP              = .TRUE. /  
  
&SURF ID              = 'PILOT '  
COLOR                = 'BLACK '
```

&OBST XB=0.0,0.0003937,0.0,0.05,0.04,0.05
SURF_ID6='MEDIUMINERT','MEDIUM','MEDIUMINERT','MEDIUMINERT'
, 'MEDIUMINERT', 'MEDIUMINERT' /

&OBST XB=0.0,0.0003937,0.0,0.05,0.06,0.07
SURF_ID6='MEDIUMINERT','MEDIUM','MEDIUMINERT','MEDIUMINERT'
, 'MEDIUMINERT', 'MEDIUMINERT' /

&OBST XB=0.0,0.0003937,0.0,0.05,0.08,0.09
SURF_ID6='MEDIUMINERT','MEDIUM','MEDIUMINERT','MEDIUMINERT'
, 'MEDIUMINERT', 'MEDIUMINERT' /

&OBST XB=0.0,0.0003937,0.0,0.05,0.1,0.11
SURF_ID6='MEDIUMINERT','MEDIUM','MEDIUMINERT','MEDIUMINERT'
, 'MEDIUMINERT', 'MEDIUMINERT' /

&OBST XB=0.0,0.0003937,0.0,0.05,0.12,0.13
SURF_ID6='MEDIUMINERT','MEDIUM','MEDIUMINERT','MEDIUMINERT'
, 'MEDIUMINERT', 'MEDIUMINERT' /

&OBST XB=0.0,0.0003937,0.0,0.05,0.14,0.15

SURF_ID6='MEDIUMINERT','MEDIUM','MEDIUMINERT','MEDIUMINERT'
, 'MEDIUMINERT', 'MEDIUMINERT' /

&OBST XB=0.0,0.0003937,0.0,0.05,0.16,0.17

SURF_ID6='MEDIUMINERT','MEDIUM','MEDIUMINERT','MEDIUMINERT'
, 'MEDIUMINERT', 'MEDIUMINERT' /

&OBST XB=0.0,0.0003937,0.0,0.05,0.18,0.19

SURF_ID6='MEDIUMINERT','MEDIUM','MEDIUMINERT','MEDIUMINERT'
, 'MEDIUMINERT', 'MEDIUMINERT' /

&OBST XB=0.0,0.0003937,0.0,0.05,0.20,0.21

SURF_ID6='MEDIUMINERT','MEDIUM','MEDIUMINERT','MEDIUMINERT'
, 'MEDIUMINERT', 'MEDIUMINERT' /

&OBST XB=0.0,0.0003937,0.0,0.05,0.22,0.23

SURF_ID6='MEDIUMINERT','MEDIUM','MEDIUMINERT','MEDIUMINERT'
, 'MEDIUMINERT', 'MEDIUMINERT' /

&VENT MB='XMIN', SURF_ID='MIRROR' /

&VENT MB='XMAX', SURF_ID='OPEN' /

&VENT MB='ZMAX', SURF_ID='OPEN' /

```
&VENT MB='ZMIN', SURF_ID='TABLE' /

&OBST XB=0.0,0.001,0.0,0.05,0.038,0.039, SURF_ID='HOT',
      DEVC_ID='TIMER1' /

&SURF ID='HOT',NO_SLIP=.TRUE.,TMP_FRONT=1000./

&DEVC ID='TIMER1',XYZ=0.0045,0.00191,0.4, SETPOINT=5,
      QUANTITY='TIME',INITIAL_STATE=.TRUE./

&SLCF PBY=0.05, QUANTITY='TEMPERATURE', VECTOR=.TRUE. /
&SLCF PBZ=0.05, QUANTITY='TEMPERATURE', VECTOR=.TRUE. /
&SLCF PBZ=0.082, QUANTITY='TEMPERATURE', VECTOR=.TRUE. /
&SLCF PBZ=0.114, QUANTITY='TEMPERATURE', VECTOR=.TRUE. /
&SLCF PBZ=0.152, QUANTITY='TEMPERATURE', VECTOR=.TRUE. /
&SLCF PBZ=0.168, QUANTITY='TEMPERATURE', VECTOR=.TRUE. /
&SLCF PBZ=0.184, QUANTITY='TEMPERATURE', VECTOR=.TRUE. /

&SLCF PBY=0.05, QUANTITY='PRESSURE' /
&SLCF PBZ=0.082, QUANTITY='PRESSURE' /
&SLCF PBZ=0.114, QUANTITY='PRESSURE' /
&SLCF PBZ=0.152, QUANTITY='PRESSURE' /
&SLCF PBZ=0.168, QUANTITY='PRESSURE' /

&SLCF PBY=0.05, QUANTITY='HRRPUV', VECTOR=.TRUE. /
```

```
&SLCF PBZ=0.05, QUANTITY='HRRPUV', VECTOR=.TRUE. /
&SLCF PBZ=0.082, QUANTITY='HRRPUV', VECTOR=.TRUE. /
&SLCF PBZ=0.114, QUANTITY='HRRPUV', VECTOR=.TRUE. /
&SLCF PBZ=0.152, QUANTITY='HRRPUV', VECTOR=.TRUE. /
&SLCF PBZ=0.168, QUANTITY='HRRPUV', VECTOR=.TRUE. /
&SLCF PBZ=0.184, QUANTITY='HRRPUV', VECTOR=.TRUE. /

&SLCF PBZ=0.05, QUANTITY='MASS FRACTION',SPEC_ID = 'OXYGEN
', VECTOR=.TRUE./
&SLCF PBZ=0.05, QUANTITY='MASS FRACTION',SPEC_ID = 'OXYGEN
', VECTOR=.TRUE./
&SLCF PBZ=0.082, QUANTITY='MASS FRACTION',SPEC_ID = '
OXYGEN', VECTOR=.TRUE./
&SLCF PBZ=0.114, QUANTITY='MASS FRACTION',SPEC_ID = '
OXYGEN', VECTOR=.TRUE./
&SLCF PBZ=0.152, QUANTITY='MASS FRACTION',SPEC_ID = '
OXYGEN', VECTOR=.TRUE./
&SLCF PBZ=0.168, QUANTITY='MASS FRACTION',SPEC_ID = '
OXYGEN', VECTOR=.TRUE./
&SLCF PBZ=0.184, QUANTITY='MASS FRACTION',SPEC_ID = '
OXYGEN', VECTOR=.TRUE./
```

```
&SLCF PBY=0.05, QUANTITY='MASS FRACTION',SPEC_ID = '
CELLULOSE', VECTOR=.TRUE./
&SLCF PBZ=0.05, QUANTITY='MASS FRACTION',SPEC_ID = '
CELLULOSE', VECTOR=.TRUE./
&SLCF PBZ=0.082, QUANTITY='MASS FRACTION',SPEC_ID = '
CELLULOSE', VECTOR=.TRUE./
&SLCF PBZ=0.114, QUANTITY='MASS FRACTION',SPEC_ID = '
CELLULOSE', VECTOR=.TRUE./
&SLCF PBZ=0.152, QUANTITY='MASS FRACTION',SPEC_ID = '
CELLULOSE', VECTOR=.TRUE./
&SLCF PBZ=0.168, QUANTITY='MASS FRACTION',SPEC_ID = '
CELLULOSE', VECTOR=.TRUE./
&SLCF PBZ=0.184, QUANTITY='MASS FRACTION',SPEC_ID = '
CELLULOSE', VECTOR=.TRUE./

&SLCF PBY=0.05, QUANTITY='MASS FRACTION',SPEC_ID = 'WATER
VAPOR', VECTOR=.TRUE./
&SLCF PBZ=0.05, QUANTITY='MASS FRACTION',SPEC_ID = 'WATER
VAPOR', VECTOR=.TRUE./
&SLCF PBZ=0.082, QUANTITY='MASS FRACTION',SPEC_ID = 'WATER
VAPOR', VECTOR=.TRUE./
&SLCF PBZ=0.114, QUANTITY='MASS FRACTION',SPEC_ID = 'WATER
VAPOR', VECTOR=.TRUE./
```

```
&SLCF PBZ=0.152, QUANTITY='MASS FRACTION', SPEC_ID = 'WATER
      VAPOR', VECTOR=.TRUE./
&SLCF PBZ=0.168, QUANTITY='MASS FRACTION', SPEC_ID = 'WATER
      VAPOR', VECTOR=.TRUE./
&SLCF PBZ=0.184, QUANTITY='MASS FRACTION', SPEC_ID = 'WATER
      VAPOR', VECTOR=.TRUE./

&SLCF PBZ=0.05, QUANTITY='MASS FRACTION', SPEC_ID = 'CARBON
      DIOXIDE', VECTOR=.TRUE./
&SLCF PBZ=0.05, QUANTITY='MASS FRACTION', SPEC_ID = 'CARBON
      DIOXIDE', VECTOR=.TRUE./
&SLCF PBZ=0.082, QUANTITY='MASS FRACTION', SPEC_ID = '
      CARBON DIOXIDE', VECTOR=.TRUE./
&SLCF PBZ=0.114, QUANTITY='MASS FRACTION', SPEC_ID = '
      CARBON DIOXIDE', VECTOR=.TRUE./
&SLCF PBZ=0.152, QUANTITY='MASS FRACTION', SPEC_ID = '
      CARBON DIOXIDE', VECTOR=.TRUE./
&SLCF PBZ=0.168, QUANTITY='MASS FRACTION', SPEC_ID = '
      CARBON DIOXIDE', VECTOR=.TRUE./
&SLCF PBZ=0.184, QUANTITY='MASS FRACTION', SPEC_ID = '
      CARBON DIOXIDE', VECTOR=.TRUE./

&BNDF QUANTITY='WALL TEMPERATURE', CELL_CENTERED=.TRUE. /
```

```
&BNDF QUANTITY='NET HEAT FLUX', CELL_CENTERED=.TRUE. /
&BNDF QUANTITY='INCIDENT HEAT FLUX', CELL_CENTERED=.TRUE.
/
&BNDF QUANTITY='BURNING RATE', CELL_CENTERED=.TRUE. /
&BNDF QUANTITY='SURFACE DENSITY', CELL_CENTERED=.TRUE. /
&BNDF QUANTITY='CONVECTIVE HEAT FLUX', CELL_CENTERED=.TRUE
. /
&BNDF QUANTITY='RADIATIVE HEAT FLUX', CELL_CENTERED=.TRUE.
/

&DUMP DT_PL3D=0.05, PLOT3D_QUANTITY(1:5)='TEMPERATURE', '
HRRPUV', 'U-VELOCITY', 'W-VELOCITY', 'MASS FRACTION',
PLOT3D_SPEC_ID(5)='OXYGEN', WRITE_XYZ=.TRUE./
&TAIL /
```

1.5-cm gap

```
fig15fp40.fds: 1cm fuel continuous run
-Symmetry plane is kept
-fuel block length 1 cm
-Separation distance: 1 cm (fuel 1cm/ air 1.5 cm,
resulting in fuel percentage of 40%)
-total of 10 fuel blocks
```

```
-Total Runtime 15s
-Oxygen Mass Fraction as Output
-Different Name convention (f1=> fuel length, g0=>
gap length, fp100=> fuel percentage)

&HEAD CHID='Discrete Run41', TITLE='Symmetric
Cardboard Setup' /

&MESH ID='cardboard', IJK=66,1,387, XB
=0.0,0.05,0.0,0.05,0.0,0.55/

&TIME T_END=12.0, WALL_INCREMENT=1 /

&DUMP DT_RESTART=1.0, NFRAMES=1100 /

&MISC BAROCLINIC=.FALSE., NOISE=.FALSE., DNS=.TRUE
./

&RADI RADIATIVE_FRACTION=0. /

&SPEC ID='NITROGEN', BACKGROUND=.TRUE./
&SPEC ID = 'CELLULOSE', FORMULA = C6H10O5, MW
=162.0/
```

```
&SPEC ID = 'OXYGEN', MASS_FRACTION_0 = 0.23/  
&SPEC ID = 'WATER VAPOR' /  
&SPEC ID = 'CARBON DIOXIDE' /  
  
&REAC FUEL          = 'CELLULOSE'  
A                  = 4.23E14  
E                  = 1.13E5  
SPEC_ID_NU        = 'CELLULOSE', 'OXYGEN', 'WATER VAPOR'  
, 'CARBON DIOXIDE'  
NU(1:4)           = -1, -6, 5, 6  
SPEC_ID_N_S       = 'CELLULOSE', 'OXYGEN'  
N_S(1:2)          = 1, 1  
HEAT_OF_COMBUSTION = 15800.  
HRRPUA_SHEET      = 1.0E10 /  
  
&MATL ID          = 'CARDBOARDMEDIUM'  
EMISSIVITY        = 1.0  
SPECIFIC_HEAT     = 1.20  
CONDUCTIVITY      = 0.06  
DENSITY           = 555.3  
  
N_REACTIONS       = 1
```

```

A(1) = 1.00E10
E(1) = 1.25E5
N_S(1) = 1.
SPEC_ID(1:4,1) = 'CELLULOSE', 'OXYGEN', '
WATER VAPOR', 'CARBON DIOXIDE'
NU_SPEC(1:4,1) = 0.9,0,0,0
NU_MATL(1,1) = 0.1
MATL_ID = 'CHARMEDIUM'
HEAT_OF_REACTION = 752.8
HEAT_OF_COMBUSTION = 15800. /

&MATL ID = 'CARDBOARDLINER'
EMISSIVITY = 1.0
SPECIFIC_HEAT = 1.20
CONDUCTIVITY = 0.06
DENSITY = 504.6 /

&MATL ID = 'CHARMEDIUM'
EMISSIVITY = 1.0
SPECIFIC_HEAT = 1.20

```

```
CONDUCTIVITY          = 0.06
DENSITY               = 555.3 /

&MATL ID              = 'STEEL'
FYI                   = '310 stainless at 320K'
EMISSIVITY            = 1.0
SPECIFIC_HEAT         = 0.48
CONDUCTIVITY          = 13.2
DENSITY               = 7870. /

&SURF ID              = 'MEDIUM'
COLOR                 = 'SIENNA'
MATL_ID               = 'CARDBOARDMEDIUM'
THICKNESS             = 0.000115
LAYER_DIVIDE         = 1.0
NO_SLIP               = .TRUE.
BACKING               = 'INSULATED' /

&SURF ID              = 'MEDIUMINERT'
COLOR                 = 'SIENNA'
MATL_ID               = 'CARDBOARDMEDIUM'
THICKNESS             = 0.000165
LAYER_DIVIDE         = 0.0
```

```
NO_SLIP                = .TRUE. /

&SURF ID                = 'LINER'
COLOR                   = 'SIENNA'
MATL_ID                 = 'CARDBOARDLINER'
THICKNESS               = 0.00041
CELL_SIZE_FACTOR       = 1000.
NO_SLIP                = .TRUE. /

&SURF ID                = 'TABLE'
COLOR                   = 'GRAY'
MATL_ID                 = 'STEEL'
THICKNESS               = 0.05
CELL_SIZE_FACTOR       = 1000.
NO_SLIP                = .TRUE. /

&SURF ID                = 'PILOT'
COLOR                   = 'BLACK'

&OBST XB=0.0,0.0003937,0.0,0.05,0.04,0.05
```

```
SURF_ID6='MEDIUMINERT','MEDIUM','MEDIUMINERT','  
MEDIUMINERT','MEDIUMINERT','MEDIUMINERT' /
```

```
&OBST XB=0.0,0.0003937,0.0,0.05,0.08,0.09
```

```
SURF_ID6='MEDIUMINERT','MEDIUM','MEDIUMINERT','  
MEDIUMINERT','MEDIUMINERT','MEDIUMINERT' /
```

```
&OBST XB=0.0,0.0003937,0.0,0.05,0.12,0.13
```

```
SURF_ID6='MEDIUMINERT','MEDIUM','MEDIUMINERT','  
MEDIUMINERT','MEDIUMINERT','MEDIUMINERT' /
```

```
&OBST XB=0.0,0.0003937,0.0,0.05,0.16,0.17
```

```
SURF_ID6='MEDIUMINERT','MEDIUM','MEDIUMINERT','  
MEDIUMINERT','MEDIUMINERT','MEDIUMINERT' /
```

```
&OBST XB=0.0,0.0003937,0.0,0.05,0.2,0.21
```

```
SURF_ID6='MEDIUMINERT','MEDIUM','MEDIUMINERT','  
MEDIUMINERT','MEDIUMINERT','MEDIUMINERT' /
```

```
&OBST XB=0.0,0.0003937,0.0,0.05,0.24,0.25
```

```
SURF_ID6='MEDIUMINERT','MEDIUM','MEDIUMINERT','  
MEDIUMINERT','MEDIUMINERT','MEDIUMINERT' /
```

```
&OBST XB=0.0,0.0003937,0.0,0.05,0.28,0.29
SURF_ID6='MEDIUMINERT','MEDIUM','MEDIUMINERT','
MEDIUMINERT','MEDIUMINERT','MEDIUMINERT' /

&OBST XB=0.0,0.0003937,0.0,0.05,0.32,0.33
SURF_ID6='MEDIUMINERT','MEDIUM','MEDIUMINERT','
MEDIUMINERT','MEDIUMINERT','MEDIUMINERT' /

&OBST XB=0.0,0.0003937,0.0,0.05,0.36,0.37
SURF_ID6='MEDIUMINERT','MEDIUM','MEDIUMINERT','
MEDIUMINERT','MEDIUMINERT','MEDIUMINERT' /

&OBST XB=0.0,0.0003937,0.0,0.05,0.4,0.41
SURF_ID6='MEDIUMINERT','MEDIUM','MEDIUMINERT','
MEDIUMINERT','MEDIUMINERT','MEDIUMINERT' /

&VENT MB='XMIN', SURF_ID='MIRROR' /
&VENT MB='XMAX', SURF_ID='OPEN' /
&VENT MB='ZMAX', SURF_ID='OPEN' /
&VENT MB='ZMIN', SURF_ID='TABLE' /

&OBST XB=0.0,0.001,0.0,0.05,0.038,0.039, SURF_ID='
HOT', DEVC_ID='TIMER1' /
```

```
&SURF ID='HOT',NO_SLIP=.TRUE.,TMP_FRONT=1000./  
&DEVC ID='TIMER1',XYZ=0.0045,0.00191,0.4, SETPOINT  
=5,QUANTITY='TIME',INITIAL_STATE=.TRUE./
```

```
&SLCF PBZ=0.05, QUANTITY='TEMPERATURE', VECTOR=.  
TRUE. /
```

```
&SLCF PBZ=0.05, QUANTITY='TEMPERATURE', VECTOR=.  
TRUE. /
```

```
&SLCF PBZ=0.082, QUANTITY='TEMPERATURE', VECTOR=.  
TRUE. /
```

```
&SLCF PBZ=0.114, QUANTITY='TEMPERATURE', VECTOR=.  
TRUE. /
```

```
&SLCF PBZ=0.152, QUANTITY='TEMPERATURE', VECTOR=.  
TRUE. /
```

```
&SLCF PBZ=0.168, QUANTITY='TEMPERATURE', VECTOR=.  
TRUE. /
```

```
&SLCF PBZ=0.184, QUANTITY='TEMPERATURE', VECTOR=.  
TRUE. /
```

```
&SLCF PBZ=0.05, QUANTITY='PRESSURE' /
```

```
&SLCF PBZ=0.082, QUANTITY='PRESSURE' /
```

```
&SLCF PBZ=0.114, QUANTITY='PRESSURE' /
```

```
&SLCF PBZ=0.152, QUANTITY='PRESSURE' /
```

```
&SLCF PBZ=0.168, QUANTITY='PRESSURE' /

&SLCF PBZ=0.05, QUANTITY='HRRPUV', VECTOR=.TRUE. /
&SLCF PBZ=0.05, QUANTITY='HRRPUV', VECTOR=.TRUE. /
&SLCF PBZ=0.082, QUANTITY='HRRPUV', VECTOR=.TRUE.

/

&SLCF PBZ=0.114, QUANTITY='HRRPUV', VECTOR=.TRUE.

/

&SLCF PBZ=0.152, QUANTITY='HRRPUV', VECTOR=.TRUE.

/

&SLCF PBZ=0.168, QUANTITY='HRRPUV', VECTOR=.TRUE.

/

&SLCF PBZ=0.184, QUANTITY='HRRPUV', VECTOR=.TRUE.

/

&SLCF PBZ=0.05, QUANTITY='MASS FRACTION', SPEC_ID =
'OXYGEN', VECTOR=.TRUE./

&SLCF PBZ=0.05, QUANTITY='MASS FRACTION', SPEC_ID =
'OXYGEN', VECTOR=.TRUE./

&SLCF PBZ=0.082, QUANTITY='MASS FRACTION', SPEC_ID
= 'OXYGEN', VECTOR=.TRUE./

&SLCF PBZ=0.114, QUANTITY='MASS FRACTION', SPEC_ID
= 'OXYGEN', VECTOR=.TRUE./
```

```
&SLCF PBZ=0.152, QUANTITY='MASS FRACTION',SPEC_ID  
= 'OXYGEN', VECTOR=.TRUE./
```

```
&SLCF PBZ=0.168, QUANTITY='MASS FRACTION',SPEC_ID  
= 'OXYGEN', VECTOR=.TRUE./
```

```
&SLCF PBZ=0.184, QUANTITY='MASS FRACTION',SPEC_ID  
= 'OXYGEN', VECTOR=.TRUE./
```

```
&SLCF PBY=0.05, QUANTITY='MASS FRACTION',SPEC_ID =  
'CELLULOSE', VECTOR=.TRUE./
```

```
&SLCF PBZ=0.05, QUANTITY='MASS FRACTION',SPEC_ID =  
'CELLULOSE', VECTOR=.TRUE./
```

```
&SLCF PBZ=0.082, QUANTITY='MASS FRACTION',SPEC_ID  
= 'CELLULOSE', VECTOR=.TRUE./
```

```
&SLCF PBZ=0.114, QUANTITY='MASS FRACTION',SPEC_ID  
= 'CELLULOSE', VECTOR=.TRUE./
```

```
&SLCF PBZ=0.152, QUANTITY='MASS FRACTION',SPEC_ID  
= 'CELLULOSE', VECTOR=.TRUE./
```

```
&SLCF PBZ=0.168, QUANTITY='MASS FRACTION',SPEC_ID  
= 'CELLULOSE', VECTOR=.TRUE./
```

```
&SLCF PBZ=0.184, QUANTITY='MASS FRACTION',SPEC_ID  
= 'CELLULOSE', VECTOR=.TRUE./
```



```
&SLCF PBZ=0.152, QUANTITY='MASS FRACTION',SPEC_ID  
= 'CARBON DIOXIDE', VECTOR=.TRUE./
```

```
&SLCF PBZ=0.168, QUANTITY='MASS FRACTION',SPEC_ID  
= 'CARBON DIOXIDE', VECTOR=.TRUE./
```

```
&SLCF PBZ=0.184, QUANTITY='MASS FRACTION',SPEC_ID  
= 'CARBON DIOXIDE', VECTOR=.TRUE./
```

```
&BNDF QUANTITY='WALL TEMPERATURE', CELL_CENTERED=  
TRUE. /
```

```
&BNDF QUANTITY='NET HEAT FLUX', CELL_CENTERED=  
TRUE. /
```

```
&BNDF QUANTITY='INCIDENT HEAT FLUX', CELL_CENTERED  
=.TRUE. /
```

```
&BNDF QUANTITY='BURNING RATE', CELL_CENTERED=.TRUE  
. /
```

```
&BNDF QUANTITY='SURFACE DENSITY', CELL_CENTERED=  
TRUE. /
```

```
&BNDF QUANTITY='CONVECTIVE HEAT FLUX',  
CELL_CENTERED=.TRUE. /
```

```
&BNDF QUANTITY='RADIATIVE HEAT FLUX',  
CELL_CENTERED=.TRUE. /
```

```
&DUMP DT_PL3D=0.05, PLOT3D_QUANTITY(1:5)='
TEMPERATURE ', 'HRRPUV ', 'U-VELOCITY ', 'W-VELOCITY ', 'MASS
FRACTION ',
PLOT3D_SPEC_ID(5)='OXYGEN', WRITE_XYZ=.TRUE./
&TAIL /
```

2 0-g Input Code

Continuous

```
!f1g0fp100_0gcg.fds: 1cm fuel continuous setup
!-Symmetry plane setup
!-fuel block length 1 cm
!-Separation distance: 0 cm (fuel 1cm/ air 0 cm,
resulting in fuel percentage of 100%)
!-total of 10 fuel blocks
!-Total Runtime 50s
!-0 gravity
!-coarse
!-20 cm/s air velocity

&HEAD CHID='microg_0cm_gap', TITLE='Symmetric
Cardboard Setup' /
```

```
&MESH ID='cardboard', IJK=66,1,387, XB
=0.0,0.05,0.0,0.05,0.0,0.55/

&TIME T_END=50, WALL_INCREMENT=1 /

&DUMP DT_RESTART=1.0, NFRAMES=1100 /

&MISC BAROCLINIC=.FALSE., NOISE=.FALSE., DNS=.TRUE
./

!Microgravity
&MISC GVEC=0,0,0/

&RADI RADIATIVE_FRACTION=0. /

&SPEC ID='NITROGEN', BACKGROUND=.TRUE./
&SPEC ID = 'CELLULOSE', FORMULA = C6H10O5, MW
=162.0/
&SPEC ID = 'OXYGEN', MASS_FRACTION_0 = 0.23/
&SPEC ID = 'WATER VAPOR' /
&SPEC ID = 'CARBON DIOXIDE' /
```

```

&REAC FUEL          = 'CELLULOSE '
A                  = 4.23E14
E                  = 1.13E5
SPEC_ID_NU        = 'CELLULOSE ', 'OXYGEN ', 'WATER VAPOR
', 'CARBON DIOXIDE '
NU(1:4)           = -1, -6, 5, 6
SPEC_ID_N_S       = 'CELLULOSE ', 'OXYGEN '
N_S(1:2)          = 1, 1
HEAT_OF_COMBUSTION = 15800.
HRRPUA_SHEET      = 1.0E10 /

&MATL ID          = 'CARDBOARDMEDIUM '
EMISSIVITY        = 1.0
SPECIFIC_HEAT     = 1.20
CONDUCTIVITY      = 0.06
DENSITY           = 555.3

N_REACTIONS       = 1
A(1)              = 1.00E10
E(1)              = 1.25E5
N_S(1)            = 1.
SPEC_ID(1:4,1)    = 'CELLULOSE ', 'OXYGEN ', '
WATER VAPOR ', 'CARBON DIOXIDE '

```

NU_SPEC(1:4,1) = 0.9,0,0,0

NU_MATL(1,1) = 0.1

MATL_ID = 'CHARMEDIUM'

HEAT_OF_REACTION = 752.8

HEAT_OF_COMBUSTION = 15800. /

&MATL ID = 'CARDBOARDLINER'

EMISSIVITY = 1.0

SPECIFIC_HEAT = 1.20

CONDUCTIVITY = 0.06

DENSITY = 504.6 /

&MATL ID = 'CHARMEDIUM'

EMISSIVITY = 1.0

SPECIFIC_HEAT = 1.20

CONDUCTIVITY = 0.06

DENSITY = 555.3 /

&MATL ID = 'STEEL'

FYI = '310 stainless at 320K'

```
EMISSIONITY          = 1.0
SPECIFIC_HEAT        = 0.48
CONDUCTIVITY         = 13.2
DENSITY              = 7870. /

&SURF ID              = 'MEDIUM'
COLOR                 = 'SIENNA'
MATL_ID               = 'CARDBOARDMEDIUM'
THICKNESS             = 0.000115
LAYER_DIVIDE         = 1.0
NO_SLIP               = .TRUE.
BACKING               = 'INSULATED' /

&SURF ID              = 'MEDIUMINERT'
COLOR                 = 'SIENNA'
MATL_ID               = 'CARDBOARDMEDIUM'
THICKNESS             = 0.000165
LAYER_DIVIDE         = 0.0
NO_SLIP               = .TRUE. /

&SURF ID              = 'LINER'
COLOR                 = 'SIENNA'
```

```
MATL_ID          = 'CARDBOARDLINER '  
THICKNESS       = 0.00041  
CELL_SIZE_FACTOR = 1000.  
NO_SLIP        = .TRUE. /  
  
&SURF ID          = 'TABLE '  
COLOR           = 'GRAY '  
MATL_ID        = 'STEEL '  
THICKNESS     = 0.05  
CELL_SIZE_FACTOR = 1000.  
NO_SLIP      = .TRUE. /  
  
&SURF ID          = 'PILOT '  
COLOR           = 'BLACK '  
  
&OBST XB=0.0,0.0003937,0.0,0.05,0.04,0.05  
SURF_ID6='MEDIUMINERT ', 'MEDIUM ', 'MEDIUMINERT ', '  
MEDIUMINERT ', 'MEDIUM ', 'MEDIUM ' /  
  
&OBST XB=0.0,0.0003937,0.0,0.05,0.05,0.06
```

```
SURF_ID6='MEDIUMINERT','MEDIUM','MEDIUMINERT','  
MEDIUMINERT','MEDIUM','MEDIUM' /
```

```
&OBST XB=0.0,0.0003937,0.0,0.05,0.06,0.07
```

```
SURF_ID6='MEDIUMINERT','MEDIUM','MEDIUMINERT','  
MEDIUMINERT','MEDIUM','MEDIUM' /
```

```
&OBST XB=0.0,0.0003937,0.0,0.05,0.07,0.08
```

```
SURF_ID6='MEDIUMINERT','MEDIUM','MEDIUMINERT','  
MEDIUMINERT','MEDIUM','MEDIUM' /
```

```
&OBST XB=0.0,0.0003937,0.0,0.05,0.08,0.09
```

```
SURF_ID6='MEDIUMINERT','MEDIUM','MEDIUMINERT','  
MEDIUMINERT','MEDIUM','MEDIUM' /
```

```
&OBST XB=0.0,0.0003937,0.0,0.05,0.09,0.10
```

```
SURF_ID6='MEDIUMINERT','MEDIUM','MEDIUMINERT','  
MEDIUMINERT','MEDIUM','MEDIUM' /
```

```
&OBST XB=0.0,0.0003937,0.0,0.05,0.10,0.11
```

```
SURF_ID6='MEDIUMINERT','MEDIUM','MEDIUMINERT','  
MEDIUMINERT','MEDIUM','MEDIUM' /
```

```
&OBST XB=0.0,0.0003937,0.0,0.05,0.11,0.12
SURF_ID6='MEDIUMINERT','MEDIUM','MEDIUMINERT','
MEDIUMINERT','MEDIUM','MEDIUM' /
```

```
&OBST XB=0.0,0.0003937,0.0,0.05,0.12,0.13
SURF_ID6='MEDIUMINERT','MEDIUM','MEDIUMINERT','
MEDIUMINERT','MEDIUM','MEDIUM' /
```

```
&OBST XB=0.0,0.0003937,0.0,0.05,0.13,0.14
SURF_ID6='MEDIUMINERT','MEDIUM','MEDIUMINERT','
MEDIUMINERT','MEDIUM','MEDIUM' /
```

```
&VENT MB='XMIN', SURF_ID='MIRROR' /
```

```
&VENT MB='XMAX', SURF_ID='OPEN' /
```

```
&VENT MB='ZMAX', SURF_ID='OPEN' /
```

```
&SURF ID = 'V_INI', SPEC_ID(1)='OXYGEN',
VOLUME_FLOW=-0.0005/
```

```
!Prescribing velocity
```

```
&VENT MB='ZMIN',
```

```
SURF_ID='V_INI' /
```

```
&OBST XB=0.0,0.001,0.0,0.05,0.038,0.039, SURF_ID='
HOT', DEVC_ID='TIMER1' /

&SURF ID='HOT',NO_SLIP=.TRUE.,TMP_FRONT=1000./

&DEVC ID='TIMER1',XYZ=0.0045,0.00191,0.4, SETPOINT
=3,QUANTITY='TIME',INITIAL_STATE=.TRUE./

&SLCF PBY=0.05, QUANTITY='TEMPERATURE', VECTOR=.
TRUE. /

&SLCF PBY=0.05, QUANTITY='PRESSURE' /

&SLCF PBY=0.05, QUANTITY='HRRPUV', VECTOR=.TRUE. /

&SLCF PBY=0.05, QUANTITY='MASS FRACTION',SPEC_ID =
'OXYGEN', VECTOR=.TRUE./

&SLCF PBY=0.05, QUANTITY='MASS FRACTION',SPEC_ID =
'CELLULOSE', VECTOR=.TRUE./

&SLCF PBY=0.05, QUANTITY='MASS FRACTION',SPEC_ID =
'WATER VAPOR', VECTOR=.TRUE./
```

```
&SLCF PBX=0.05 , QUANTITY='MASS FRACTION' ,SPEC_ID =
'CARBON DIOXIDE' , VECTOR=.TRUE./

&BNDF QUANTITY='WALL TEMPERATURE' , CELL_CENTERED=.
TRUE. /

&BNDF QUANTITY='NET HEAT FLUX' , CELL_CENTERED=.
TRUE. /

&BNDF QUANTITY='INCIDENT HEAT FLUX' , CELL_CENTERED
=.TRUE. /

&BNDF QUANTITY='BURNING RATE' , CELL_CENTERED=.TRUE
. /

&BNDF QUANTITY='SURFACE DENSITY' , CELL_CENTERED=.
TRUE. /

&BNDF QUANTITY='CONVECTIVE HEAT FLUX' ,
CELL_CENTERED=.TRUE. /

&BNDF QUANTITY='RADIATIVE HEAT FLUX' ,
CELL_CENTERED=.TRUE. /

&DUMP DT_PL3D=0.05 , PLOT3D_QUANTITY(1:5)='
TEMPERATURE' , 'HRRPUV' , 'U-VELOCITY' , 'W-VELOCITY' , 'MASS
FRACTION' ,

PLOT3D_SPEC_ID(5)='OXYGEN' , WRITE_XYZ=.TRUE./
```

```
&TAIL /
```

1.5-cm gap

```
!fig1_5fp40_0gcg.fds: 1cm fuel discrete run with  
1.5cm gap
```

```
!-Symmetry plane setup
```

```
!-fuel block length 1 cm
```

```
!-Separation distance: 1.5 cm (fuel 1cm/ air 1.5  
cm, resulting in fuel percentage of 40%)
```

```
!-total of 10 fuel blocks
```

```
!-Total Runtime 50s
```

```
!-0 gravity
```

```
!-coarse grid
```

```
!-20 cm/s air velocity
```

```
&HEAD CHID='microg_1_5cm_gap', TITLE='Symmetric  
Cardboard Setup' /
```

```
&MESH ID='cardboard', IJK=66,1,387, XB  
=0.0,0.05,0.0,0.05,0.0,0.55/
```

```
&TIME T_END=50, WALL_INCREMENT=1 /
```

```
&DUMP DT_RESTART=1.0, NFRAMES=1100 /

&MISC BAROCLINIC=.FALSE., NOISE=.FALSE., DNS=.TRUE
./

!Microgravity
&MISC GVEC=0,0,0/

&RADI RADIATIVE_FRACTION=0. /

&SPEC ID='NITROGEN', BACKGROUND=.TRUE./
&SPEC ID = 'CELLULOSE', FORMULA = C6H10O5, MW
=162.0/
&SPEC ID = 'OXYGEN', MASS_FRACTION_0 = 0.23/
&SPEC ID = 'WATER VAPOR' /
&SPEC ID = 'CARBON DIOXIDE' /

&REAC FUEL          = 'CELLULOSE'

A          = 4.23E14
E          = 1.13E5

SPEC_ID_NU      = 'CELLULOSE', 'OXYGEN', 'WATER VAPOR
', 'CARBON DIOXIDE'
```

```
NU(1:4)          = -1, -6, 5, 6
SPEC_ID_N_S     = 'CELLULOSE', 'OXYGEN'
N_S(1:2)        = 1, 1
HEAT_OF_COMBUSTION = 15800.
HRRPUA_SHEET    = 1.0E10 /

&MATL ID                               = 'CARDBOARDMEDIUM'
EMISSIONITY                               = 1.0
SPECIFIC_HEAT                               = 1.20
CONDUCTIVITY                               = 0.06
DENSITY                               = 555.3

N_REACTIONS                               = 1
A(1)                                       = 1.00E10
E(1)                                       = 1.25E5
N_S(1)                                       = 1.
SPEC_ID(1:4,1)                             = 'CELLULOSE', 'OXYGEN', '
WATER VAPOR', 'CARBON DIOXIDE'
NU_SPEC(1:4,1)                             = 0.9,0,0,0
NU_MATL(1,1)                               = 0.1
MATL_ID                                       = 'CHARMEDIUM'
HEAT_OF_REACTION                             = 752.8
HEAT_OF_COMBUSTION                             = 15800. /
```

```
&MATL ID                = 'CARDBOARDLINER'  
EMISSIONIVITY           = 1.0  
SPECIFIC_HEAT           = 1.20  
CONDUCTIVITY            = 0.06  
DENSITY                  = 504.6 /
```

```
&MATL ID                = 'CHARMEDIUM'  
EMISSIONIVITY           = 1.0  
SPECIFIC_HEAT           = 1.20  
CONDUCTIVITY            = 0.06  
DENSITY                  = 555.3 /
```

```
&MATL ID                = 'STEEL'  
FYI                     = '310 stainless at 320K'  
EMISSIONIVITY           = 1.0  
SPECIFIC_HEAT           = 0.48  
CONDUCTIVITY            = 13.2  
DENSITY                  = 7870. /
```

```
&SURF ID          = 'MEDIUM'
COLOR             = 'SIENNA'
MATL_ID          = 'CARDBOARDMEDIUM'
THICKNESS        = 0.000115
LAYER_DIVIDE     = 1.0
NO_SLIP          = .TRUE.
BACKING          = 'INSULATED' /

&SURF ID          = 'MEDIUMINERT'
COLOR             = 'SIENNA'
MATL_ID          = 'CARDBOARDMEDIUM'
THICKNESS        = 0.000165
LAYER_DIVIDE     = 0.0
NO_SLIP          = .TRUE. /

&SURF ID          = 'LINER'
COLOR             = 'SIENNA'
MATL_ID          = 'CARDBOARDLINER'
THICKNESS        = 0.00041
CELL_SIZE_FACTOR = 1000.
NO_SLIP          = .TRUE. /
```

```
&SURF ID                      = 'TABLE '  
COLOR                          = 'GRAY '  
MATL_ID                        = 'STEEL '  
THICKNESS                      = 0.05  
CELL_SIZE_FACTOR              = 1000.  
NO_SLIP                        = .TRUE. /  
  
&SURF ID                      = 'PILOT '  
COLOR                          = 'BLACK '  
  
&OBST XB=0.0,0.0003937,0.0,0.05,0.04,0.05  
SURF_ID6='MEDIUMINERT ','MEDIUM ','MEDIUMINERT ','  
MEDIUMINERT ','MEDIUM ','MEDIUM ' /  
  
&OBST XB=0.0,0.0003937,0.0,0.05,0.065,0.075  
SURF_ID6='MEDIUMINERT ','MEDIUM ','MEDIUMINERT ','  
MEDIUMINERT ','MEDIUM ','MEDIUM ' /  
  
&OBST XB=0.0,0.0003937,0.0,0.05,0.09,0.1  
SURF_ID6='MEDIUMINERT ','MEDIUM ','MEDIUMINERT ','  
MEDIUMINERT ','MEDIUM ','MEDIUM ' /
```

```
&OBST XB=0.0,0.0003937,0.0,0.05,0.115,0.125
SURF_ID6='MEDIUMINERT','MEDIUM','MEDIUMINERT','
MEDIUMINERT','MEDIUM','MEDIUM' /
```

```
&OBST XB=0.0,0.0003937,0.0,0.05,0.14,0.15
SURF_ID6='MEDIUMINERT','MEDIUM','MEDIUMINERT','
MEDIUMINERT','MEDIUM','MEDIUM' /
```

```
&OBST XB=0.0,0.0003937,0.0,0.05,0.165,0.175
SURF_ID6='MEDIUMINERT','MEDIUM','MEDIUMINERT','
MEDIUMINERT','MEDIUM','MEDIUM' /
```

```
&OBST XB=0.0,0.0003937,0.0,0.05,0.19,0.2
SURF_ID6='MEDIUMINERT','MEDIUM','MEDIUMINERT','
MEDIUMINERT','MEDIUM','MEDIUM' /
```

```
&OBST XB=0.0,0.0003937,0.0,0.05,0.215,0.225
SURF_ID6='MEDIUMINERT','MEDIUM','MEDIUMINERT','
MEDIUMINERT','MEDIUM','MEDIUM' /
```

```
&OBST XB=0.0,0.0003937,0.0,0.05,0.24,0.25
```

```
SURF_ID6='MEDIUMINERT', 'MEDIUM', 'MEDIUMINERT', 'MEDIUMINERT', 'MEDIUM', 'MEDIUM' /
```

```
&OBST XB=0.0,0.0003937,0.0,0.05,0.265,0.275
```

```
SURF_ID6='MEDIUMINERT', 'MEDIUM', 'MEDIUMINERT', 'MEDIUMINERT', 'MEDIUM', 'MEDIUM' /
```

```
&VENT MB='XMIN', SURF_ID='MIRROR' /
```

```
&VENT MB='XMAX', SURF_ID='OPEN' /
```

```
&VENT MB='ZMAX', SURF_ID='OPEN' /
```

```
&SURF ID = 'V_INI', SPEC_ID(1)='OXYGEN',  
VOLUME_FLOW=-0.0005/
```

```
!Prescribing velocity
```

```
&VENT MB='ZMIN',
```

```
SURF_ID='V_INI' /
```

```
&OBST XB=0.0,0.001,0.0,0.05,0.038,0.039, SURF_ID='HOT',  
DEVC_ID='TIMER1' /
```

```
&SURF ID='HOT', NO_SLIP=.TRUE., TMP_FRONT=1000. /
```

```
&DEVC ID='TIMER1',XYZ=0.0045,0.00191,0.4, SETPOINT
=3,QUANTITY='TIME',INITIAL_STATE=.TRUE./
```

```
&SLCF PBY=0.05, QUANTITY='TEMPERATURE', VECTOR=.
TRUE. /
```

```
&SLCF PBY=0.05, QUANTITY='PRESSURE' /
```

```
&SLCF PBY=0.05, QUANTITY='HRRPUV', VECTOR=.TRUE. /
```

```
&SLCF PBY=0.05, QUANTITY='MASS FRACTION',SPEC_ID =
'OXYGEN', VECTOR=.TRUE./
```

```
&SLCF PBY=0.05, QUANTITY='MASS FRACTION',SPEC_ID =
'CELLULOSE', VECTOR=.TRUE./
```

```
&SLCF PBY=0.05, QUANTITY='MASS FRACTION',SPEC_ID =
'WATER VAPOR', VECTOR=.TRUE./
```

```
&SLCF PBY=0.05, QUANTITY='MASS FRACTION',SPEC_ID =
'CARBON DIOXIDE', VECTOR=.TRUE./
```

```
&BNDF QUANTITY='WALL TEMPERATURE', CELL_CENTERED=.
TRUE. /

&BNDF QUANTITY='NET HEAT FLUX', CELL_CENTERED=.
TRUE. /

&BNDF QUANTITY='INCIDENT HEAT FLUX', CELL_CENTERED
=.TRUE. /

&BNDF QUANTITY='BURNING RATE', CELL_CENTERED=.TRUE
. /

&BNDF QUANTITY='SURFACE DENSITY', CELL_CENTERED=.
TRUE. /

&BNDF QUANTITY='CONVECTIVE HEAT FLUX',
CELL_CENTERED=.TRUE. /

&BNDF QUANTITY='RADIATIVE HEAT FLUX',
CELL_CENTERED=.TRUE. /

&DUMP DT_PL3D=0.05, PLOT3D_QUANTITY(1:5)='
TEMPERATURE', 'HRRPUV', 'U-VELOCITY', 'W-VELOCITY', 'MASS
FRACTION',
PLOT3D_SPEC_ID(5)='OXYGEN', WRITE_XYZ=.TRUE./

&TAIL /
```

Complete References

- [1] J. Q. Quintiere, C. H. Lee, "Ignitor and Thickness Effects on Upward Flame Spread," *Fire Technology*, vol. 34, no. 1, 1998.
- [2] K. Saito, J. G. Quintiere, F. A. Williams. "Upward Turbulent Flame Spread." *Fire Saf Sci; Proceedings of the First International Symposium*, 1985, p. 75-86.
- [3] J. L. Consalvi, Y. Pizzo, B. Porterie and J.L. Torero, "On the Flame Height Definition for Upward Flame Spread," *Fire Safety Journal*, Vol. 42, No. 5, pp. 384-392, 2007
- [4] A. Fernandez-Pello. The Solid Phase. In: Cox G editor. *Combustion Fundamentals of Fire*. Academic Press, San Diego, 1995, pp. 31-100.
- [5] A. C. Fernandez-Pello , T. Hirano, "Controlling Mechanisms of Flame Spread." *textit-Combust Sci Technol* vol. 32, pp. 1-31, 1983.
- [6] J. L. Consalvi, Y. Pizzo, B. Porterie and J.L. Torero, "On the Flame Height Definition for Upward Flame Spread", *textitFire Safety Journal* 42 (5) pp. 384-392, 2007
- [7] A. C. Fernandez-Pello. "Flame Spread Modeling." *Combust Sci Technol* 1984;39:119-134.
- [8] H. T. Syuhei Abe, Akihiko Ito, "Flame spread along a thin combustible solid with randomly distributed square pores of two different sizes," *Modern Applied Science*, vol. 6, no. 9, 2012.
- [9] E. Stalkup, "Numerical Modeling of Upward Flame Spread and Burning of Wavy Thin Solids", MS Thesis, Case Western Reserve University, 2014.
- [10] R. G. Rehm and H. R. Baum, "The equations of motion for thermally driven, buoyant flows," *Journal of Research of the NBS*, vol. 83, pp. 297-308, 1978.
- [11] Y. Watanabe et al: Flame Spread along a Thin Solid Randomly Distributed Combustible and Noncombustible Areas, *Proceedings of the Combustion Institute*, Vol. 33, pp, 2449-2455, 2011
- [12] M. J. Goller, et al: Burning Behavior of Vertical Matchstick Arrays, *Combustion Science and Technology*, Vol. 184, pp. 585-607, 2012
- [13] M. F. Wolff et al: Wind-Aided Firespread across Arrays of Discrete Fuel Elements. II. Experiment, *Combustion Science and Technology*, Vol. 77, pp. 261-289, 1991

- [14] C. H. Miller and M. J. Gollner: Upward Flame Spread over Discrete Fuels, 9th U.S. National Combustion Meeting, Cincinnati Ohio, May 17-20, 2015
- [15] M. Vogel and F. A. Williams: Flame Propagation along Matchstick Arrays, *Combustion Science and Technology*, Vol. 1, pp. 429-436, 1970
- [16] J. M. Prahl and J. S. T'ien: Preliminary Investigations of Forced Convection on Flame Propagation along Paper and Matchstick Arrays, *Combustion Science and Technology*, Vol. 7, pp. 271-282, 1973
- [17] R. O. Weber: A Model for Fire Propagation in Arrays, *Mathematical and Computer Modelling*, Vol. 3, No. 12, pp. 95-102, 1990
- [18] M. A. Finney et al: An Examination of Fire Spread Thresholds in Discontinuous Fuel Beds, *International Journal of Wildland Fire*, Vol. 19, pp. 163-170, 2010
- [19] Y.-T. Liao and J. S. T'ien: A Numerical Simulation of Transient Ignition and Ignition Limit of a Composite Solid by a localised radiant source 2013
- [20] National Institute of Standards and Technology, Gaithersburg, MD, USA, and VTT Technical Research Centre of Finland, Espoo, Finland, *Fire Dynamics Simulator (Version 6) Technical Reference Guide*, NIST Special Publication 1018-1, 6th ed., Apr. 13, 2015.
- [21] R. J. McDermott, "A velocity divergence constraint for large-eddy simulation of low-Mach flows," *Journal of Computational Physics*, vol. 274, pp. 413-431, 2014.
- [22] <https://www.youtube.com/watch?v=okdzskdlhtc&feature=youtu.be>
- [23] <https://www.youtube.com/watch?v=3Brup5C2EiY&feature=youtu.be>
- [24] Y. -T. Tseng, "Three-dimensional model of solid ignition and ignition limit by a non-uniformly distributed radiant heat source," PhD Thesis, Case Western Reserve University, 2011.
- [25] M. M. Khan, K. L. T. Jamison, and J. L. de Ris, "Upward fire growth over thermally thin corrugated paperboard," *textitFire Safety Science*, vol. 10, pp. 513-526, 2011.
- [26] K. J. Overholt, M. J. Gollner, J. Perricone, A. S. Rangwala, and F. A. Williams, "Warehouse commodity classification from fundamental principles. Part II: Flame heights and flame spread," *textitFire Safety Journal*, vol. 46, pp. 317-329, 6 2011.
- [27] D. Twede and S. E. M. Selke, *Cartons, textitCrates and Corrugated Board*, Handbook of Paper and Wood Packaging Technology. DEStech Publications, Inc, 2005.

- [28] P. V. Ferkul, "A model of concurrent flow flame spread over a thin solid fuel," PhD Thesis, Case Western Reserve University, 1993.
- [29] R. Seballous, J. Brucker, " Upward Flame Spread Over an Array of Discrete Fuel Elements," Senior Project Report, Case Western Reserve University, 2017.